



Quaternary geology of Long Island (Bahamas): an alternative perception of Bahamian island formation and relative sea-level changes in this area during the Last Interglacial

Lucas Vimpere ^{a,*} , Pascal Kindler ^a, Nabil A. Shawwa ^b , Giovan Peyrotty ^a, Sébastien Castelltort ^a

^a Department of Earth Sciences, University of Geneva, Rue des Maréchaux 13, 1205, Geneva, Switzerland

^b Department of Earth Sciences, Carleton University, 1125 Colonel by Drive, Ottawa, ON, K1S 5B6, Canada

ARTICLE INFO

Handling Editor: I Hendy

Keywords:

The Bahamas
Long Island
Stratigraphy
Island formation
Last interglacial
Sea-level changes

ABSTRACT

Relying on a multi-method approach including morphostratigraphy, sedimentology, petrology, and Sr-isotope, U-Th, amino-acid racemization and ^{14}C dating, we have identified, described, and mapped eight allostratigraphic units on Long Island (NE Bahamas). These units mostly consist of eolianites, but locally include reefal and sandy coastal deposits. They range in age from the middle Pleistocene to the late Holocene, are usually separated by *terra-rossa* paleosols, and can generally be correlated with the members and formations previously defined on other Bahamian islands. However, the Buckley Settlement and the Dean's Bay units, respectively equivalents of the mid-Holocene North Point Member and of the late Pleistocene Whale Point Formation, are more widespread on Long Island than on other islands, possibly due to a difference in the width of the windward shelf. Furthermore, we could not identify on Long Island a counterpart of the French Bay Member, an extensive rock body supposedly accumulated during the transgression at the onset of the last interglacial period (LIG). The lack of such deposits brings about questions about the volume and the nature of transgressive sediments that can possibly be preserved during a sea-level cycle in the Bahamas, and leads us to reconsider previously proposed models of Bahamian island development. Finally, the examination and, in some cases, the dating of paleo sea-level markers of LIG age suggest that RSL on Long Island was about +3 m above modern datum in the first half of the LIG, and rose to about +5 m in the middle of this period. This rise was likely not preceded by an exposure event.

1. Introduction

For long, the study of the rock bodies exposed on the Bahamas Islands lagged behind that of modern sediments lying on the adjacent submerged banks. Stratigraphic research in this area mostly began in the early 1980's. The first investigations focused on the most accessible places such as New Providence (Garrett and Gould, 1984; Hearty and Kindler, 1997), Eleuthera (Kindler and Hearty, 1995; Hearty, 1998), and San Salvador (Titus, 1980, 1983; Carew and Mylroie, 1985). In fact, the first stratigraphic schemes pertaining to the Bahamas archipelago were largely derived from observations made on San Salvador (Carew and Mylroie, 1985, 1995a; Hearty and Kindler, 1993a), likely because of the facilities provided by the presence of the Bahamian Field Station (now Gerace Research Center) on this island. The geology of these islands was

then complemented during the first decades of this century (e.g., Reid, 2010; Muhs et al., 2020; Nolting et al., 2023), while stratigraphic research expanded to more remote places such as the Exumas (Jackson, 2017; Hearty and Backstrom, 2021), Mayaguana (Godefroid, 2011), Crooked (Godefroid and Kindler, 2016), and West Caicos (Kerans et al., 2019). However, apart from the study of Hearty (2010), no extensive stratigraphic investigation has yet been carried out on Long Island, one of the largest land masses in the Bahamas.

Neumann and Moore (1975) were the first geologists working in the Bahamas to identify fossil tidal notches and sea caves 4–6 m above modern sea level as formed during the last interglacial period (LIG, Marine Isotope Stage 5e, ca. 128–116 ka BP, Stirling et al., 1998). Subsequently, reconstructing the relative sea-level (RSL) record of the LIG from Bahamian rocks became a prime target for many researchers (e.g.,

* Corresponding author.

E-mail address: Lucas.Vimpere@unige.ch (L. Vimpere).

Hattin and Warren, 1989; Chen et al., 1991; Neumann and Hearty, 1996; Hearty and Neumann, 2001; Thompson et al., 2011; Skrivanek et al., 2018; Kerans et al., 2019; Muhs et al., 2020; Dyer et al., 2021; Dumitru et al., 2023; Fouke and Kerans, 2024) because this period is commonly regarded as one of the best analogues for a future warmer world (Clark and Huybers, 2009). Despite all these efforts, several uncertainties still remain regarding the number of fluctuations and maximum elevation of

sea level during the LIG. In particular, a major divergence persists regarding the presence or absence of a sea-level fall in the middle of Marine Isotope Stage (MIS) 5e (e.g., Neumann and Hearty, 1996; Blanchon et al., 2009; Kopp et al., 2013; Barlow et al., 2018).

The aims of this paper are thus the following. First, we present a detailed description of the rock bodies exposed on Long Island, and provide a map showing their spatial distribution. We then compare the

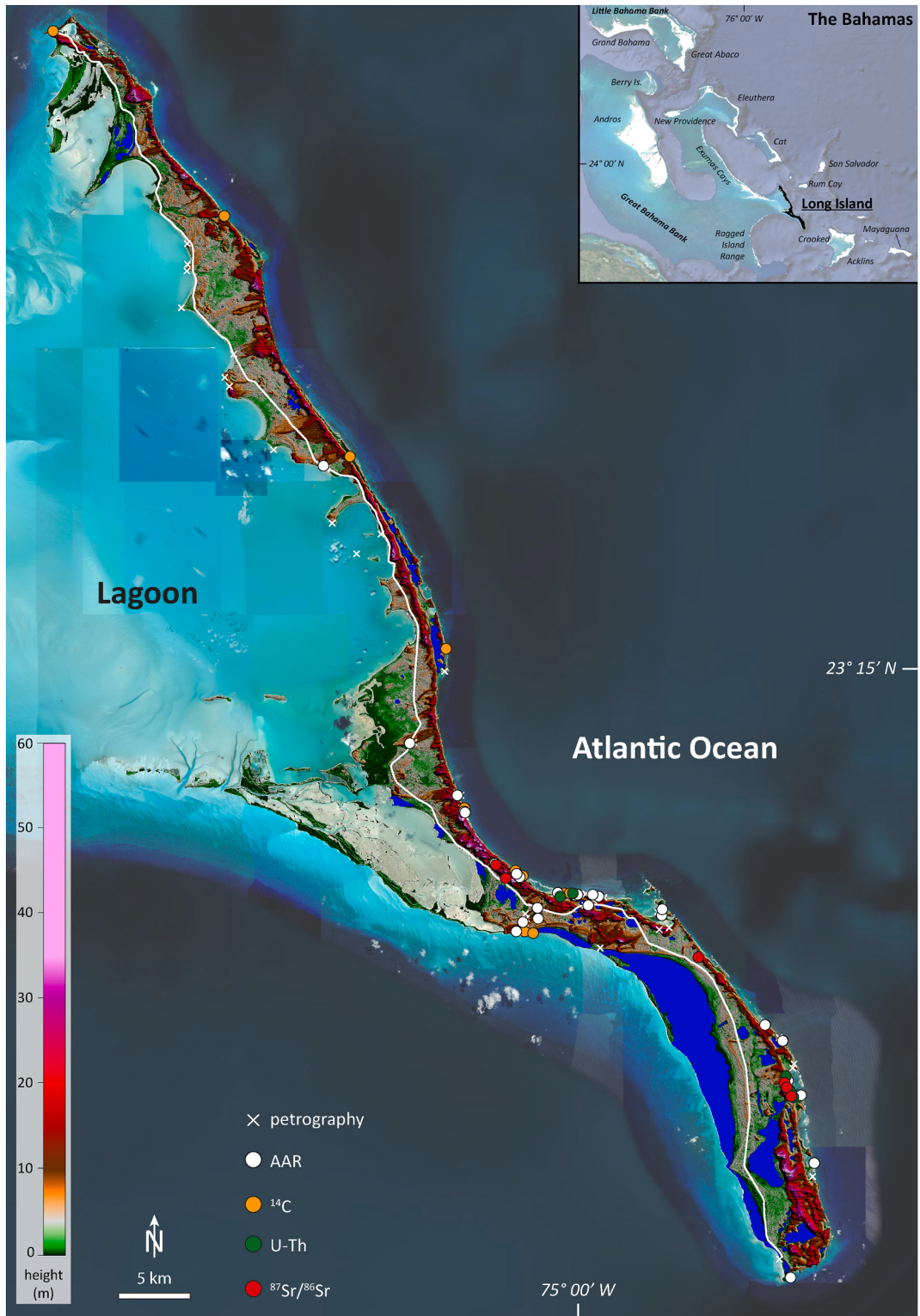


Fig. 1. Inset map shows the major carbonate banks and islands of the Bahamas. Main map is the TanDEM-X DEM of Long Island used for morphostratigraphic mapping that locates the sampling sites from this study.

stratigraphy of this island with that of the rest of the archipelago, and discuss the depositional model most frequently applied to the Quaternary geology of the Bahamas (e.g., Carew and Mylroie, 1995a, 1997; Curran et al., 2004; Mylroie, 2008). Secondly, based on the RSL markers of LIG age observed on Long Island, we provide supplementary elements regarding the sea-level history in this area during MIS 5e.

2. Background information

2.1. Geographic and tectonic settings

The Bahamas Islands embrace a ca. 1'000 km-long portion of a NW-SE trending archipelago that extends from off the eastern coast of Florida to just off the coast of Cuba (Fig. 1). The archipelago stretches out farther towards the southeast as the Turks and Caicos Islands, a distinct political entity. The modern topography of the Bahamas is characterized by two distinct realms: the flat-top, steep-sided platforms, or banks, and the deep-water troughs. The banks have been sites of shallow-water carbonate deposition since at least the early Cretaceous (Lynts, 1970). The deep-water realm comprises channels and re-entrants, together with the peri-platform ocean. These oceanic troughs isolate the banks from siliciclastic input, with the exception of airborne dust from the Sahara (Muhs et al., 1990), making them an almost pure carbonate system. Located in the northern portion of the archipelago, Great Bahama Bank (GBB) and Little Bahama Bank (LBB) are the largest edifices of which only a fraction emerges as narrow and elongated windward islands. Smaller banks (e.g., San Salvador, Inagua, and Mayaguana) lie in the southern part of the region, and are almost entirely covered by a land mass. High-energy environments prevail along the windward shorelines, whereas leeward coasts experience quiet lagoonal conditions. Long Island is a NW-SE trending, 105 km-long, 6 km-wide island that comprises the southeastern tip of GBB (Fig. 1). Cliffs and steep headlands are common along the northern shorelines, whereas the southern part of the island shows a gentler topography with extensive sandy beaches and wetlands (Sealey and Logan, 2019).

Early workers (e.g., Meyerhoff and Hatten, 1974; Mullins and Lynts, 1977) assumed a continental basement for the Bahamas, but it is now admitted that the northern part of archipelago rests on the stretched continental crust of the North American plate, whereas its southern part overlies volcanically-thickened oceanic crust related to the Triassic-Jurassic Bahamas hotspot (Shipper and Mann, 2024). Most studies (e.g., Uchupi et al., 1971; Mullins and Lynts, 1977; Carew and Mylroie, 1995b) praise the tectonic stability, or slow subsidence of the region. However, relying on the examination of shallow cores, Pierson (1982) remarked that all banks do not move downwards at the same rate. GBB, including Long Island, appears to subside at a rate of about 14 mm/10³ yrs, whereas the subsidence rate of LBB is about half of this value. Furthermore, the paradigm of regional tectonic stability has been challenged by investigations conducted both in the northwestern (Masaferro et al., 1999; Mulder et al., 2012) and southeastern (Kindler et al., 2011) parts of the archipelago, the latter standing less than 100 km to the north of the oblique convergence zone between the North American and the Caribbean plates (Dolan et al., 1998).

2.2. Stratigraphic models applied to the Bahamas

The Bahamas islands consist of vertically stacked and/or laterally juxtaposed carbonate units, mostly eolianites, separated by thin red to brown layers corresponding to paleosols. The generally accepted glacio-eustatic model, initially developed from observations made in Bermuda (Bretz, 1960; Land et al., 1967; Vacher and Rowe, 1997), asserts that carbonate deposits accumulate during interglacial highstands, when the platform tops are partially flooded by shallow waters, whereas paleosols essentially form during glacial lowstands, when the banks are subaerially exposed. According Carew and Mylroie (1995a, 1997), carbonate packages deposited during interglacial periods comprise three parts: a

transgressive phase, a stillstand phase, and a regressive phase. These phases each contain subtidal, intertidal and eolian sediments, the latter ones being in general most extensively represented, especially in the transgressive phase. Deposits of each phase allegedly present distinctive sedimentological characteristics (e.g., preservation of fine-scale eolian structures, abundance of plant remains; occurrence of interstratified protosols; Carew and Mylroie, 1997) that facilitate their recognition in the field.

2.3. Bahamian stratigraphic units

2.3.1. The Owl's Hole Formation (OHF; Carew and Mylroie, 1985)

The OHF includes several deeply karstified, paleosol-capped bioclastic and oolitic-peloidal calcarenite units deposited in eolian and, to a lesser extent, shallow-marine settings. Tentative U-Th dating of whole-rock samples gave ages of ca. 200 ka BP (Muhs and Bush, 1987) and 316 ka BP (Kindler et al., 2007). This age range is further supported by amino-acid racemization (AAR) data from these rocks that encompass Aminozones F/G to I (Hearty and Kaufman, 2000, 2009), and by four ⁸⁷Sr/⁸⁶Sr values obtained from exposures of this formation on Mayaguana averaging at 0.709155 (0.34–0.88 Ma, Kindler et al., 2011). The OHF thus comprises deposits formed during interglacial highstands of the middle Pleistocene, spanning MIS 7 to possibly MIS 15 (Hearty and Kaufman, 2000, 2009). It is identifiable by its position below or landward of the Grotto Beach Formation (see next section) and by its high degree of diagenetic alteration at all scales compared to younger units.

2.3.2. The Grotto Beach Formation (GBF; Carew and Mylroie, 1985)

This GBF is the most conspicuous stratigraphic unit in the Bahamas, forming some of the highest elevations of the archipelago and blanketing many islands. It has long been correlated with the LIG, and was subdivided into two members by Carew and Mylroie (1985): (1) the French Bay Member (FBM), and (2) the Cockburn Town Member (CTM).

The FBM is made of a well-preserved oolite commonly showing pristine sedimentary structures typical of the eolian depositional environment. It has been interpreted as the transgressive-phase deposits of the GBF (Carew and Mylroie, 1985), and alternatively, as representing an early highstand phase during MIS 5e (Hearty and Kindler, 1993a). The FBM has been attributed to the early part of the LIG based on AAR data indicating Aminozone E2 (Hearty and Kaufman, 2000, 2009).

The CTM comprises coral boundstone/rudstone and shell-rich floatstone, formed in reefal and lagoonal settings, respectively. The latter facies commonly covers the interior of many islands. U-Th ages obtained from well-preserved coral samples generally indicate two phases of reef growth between ca. 129.8 to 124.5 ka BP and ca. 123.6 to 119.4 ka BP, respectively (Chen et al., 1991; Thompson et al., 2011; Skrivanek et al., 2018). AAR data obtained on samples collected from the rudstone matrices indicate Aminozone E1 (Hearty and Kaufman, 2000, 2009). At many localities, predominantly oolitic calcarenites, displaying a shallowing-upward succession of facies from subtidal to eolian, conformably overlie the aforementioned reefal facies. These rocks were lumped into the CTM and interpreted as the regressive-phase deposits of the GBF by Carew and Mylroie (1985). Other authors regard these calcarenites as a separate entity (Fernandez Bay Member, Hearty and Kindler, 1993a; Big Cove Member, Godefroid, 2011) corresponding to a late MIS 5e highstand.

2.3.3. The Whale Point Formation (WPF; Kindler and Hearty, 2022)

First identified on San Salvador Island (Almgreen Cay Formation; Hearty and Kindler, 1993a), this unit includes rhizomorph-rich, paleosol-capped, well-preserved bioclastic eolianites forming coastal bluffs and headlands located close to the platform margin, and overlying or juxtaposed to the GBF. The occurrence of a paleosol and/or a calcrete at the base and at the top of this unit clearly shows that it post-dates the GBF, but predates the Rice Bay Formation (see next section). AAR data obtained from whole-rock samples collected from these calcarenites

indicate Aminozone C (Hearty and Kaufman, 2000, 2009), suggesting a correlation with MIS 5a (88–74 ka BP; Lisiecki and Raymo, 2005).

2.3.4. The Rice Bay Formation (RBF; Carew and Mylroie, 1985)

The RBF generally occurs at the present shoreline, and is correlated with the Holocene. It may overlie any paleosol-capped unit (usually the GBF), but is itself only covered by a mm-thin micritic crust or a modern soil. This unit comprises two members defined by Carew and Mylroie (1985): (1) the *North Point Member* (NPM) and (2) the *Hanna Bay Member* (HBM).

The NPM consists of transgressive-phase oolitic-peloidal eolianites displaying pristine structures occurring all the way down to modern sea level and below. These rocks differ petrographically from those forming the FBM by the occurrence of many thinly-coated grains and more abundant peloids and bioclasts (Kindler and Hearty, 1996). Most recent ^{14}C data obtained from whole-rock samples and *Cerion* sp. shells suggest these sediments were formed on the shallow platforms around 6.2 ka BP, and deposited on the islands in the next 1'000 years or less (Hearty and Kaufman, 2009).

The HBM is predominantly represented by bioclastic calcarenites deposited in a beach-dune environment, usually in equilibrium with modern sea level. However, at some sites (e.g., Joulter's Cay; Halley and Harris, 1979), this unit consists of oolitic grainstone. Recently obtained ^{14}C ages (Hearty and Kaufman, 2009) show that these sediments were generated between 4.7 and 3.8 ka ago. A model accounting for the depositional break between the two members of the RBF and for their distinctive petrographic composition has been presented by Kindler (1992).

2.4. Previous work on the surficial geology of long island

As mentioned above, investigations concerned with the surface geology of Long Island are scarce. Mylroie et al. (1991) surveyed a few karstic caves in the area, and discussed the relationship between the timing of their formation and the sea-level fluctuations of the late Pleistocene. However, these authors did not pay much attention to the encasing bedrock. Curran et al. (2004) published a fieldtrip guide concerning nine sites located around Stella Maris in the northern portion of the island. They applied the stratigraphic model developed on San Salvador by Carew and Mylroie (1985, 1995a, 1997), and only report on exposures of Holocene (HBM, NPM) and upper Pleistocene (GBF) rocks without presenting any geochronological and microfacies data. Hearty's (2010) study essentially focuses on the evolution of *Cerion* sp. land snail over the past 130 kyr, but also proposes a chronostratigraphic scheme for the island. Relying on whole-rock AAR data, this author recognized five calcarenite units spanning the interval from the middle Pleistocene to the Holocene, and correlated them with the stratigraphy established on San Salvador by Hearty and Kindler (1993a). However, this work does not present a geological map of Long Island, and lacks detailed petrographic and sedimentological descriptions of the various units. Vimpere (2017) studied the geology around and within Dean's Blue Hole (southern part of the island). The data of this unpublished master's thesis are incorporated in the present paper. Vimpere et al. (2019, 2021) integrated exposures from Long Island in an archipelago-wide study of parabolic dunes, and Dyer et al. (2021) did the same in a compilation of sea-level markers across the Bahamas to better constrain the peak LIG ice melt. Dyer et al. (2021) also produced a geologic map of Long Island delineating Holocene sediments, LIG flats, and dunes of unspecified age. Finally, Dumitru et al. (2023) provided high-precision U-Th data from four reef of MIS 5e age located in the southern part of the island, but did not give detailed information on the setting of these buildups.

3. Methods

3.1. Morphostratigraphy

A combination of satellite images and digital elevation model was used to generate the base-map of Long Island and to identify the main geomorphic units. The TanDEM-X digital elevation model (DEM) used in this study is provided by the German Aerospace Centre (DLR) at 0.4 arcsec at the equator (*ca.* 12 m) with a relative vertical accuracy of ± 2 m (Wessel et al., 2018). We applied a constant vertical offset of +34.1 m to the raw TanDEM-X elevations to effectively reference them to present-day mean sea level (MSL). This offset is consistent with the calibration reported by Dyer et al. (2021) in central Long Island, where MSL was measured at -33.96 m relative to the TanDEM-X reference via EGM2008 geoid correction. Nonetheless, the authors noted that MSL varies by more than a meter across the island. We combined it with the raw dataset ± 2 m accuracy to adopt a conservative vertical uncertainty of ± 3 m. We applied the morphostratigraphic principles of lateral accretion (Itzhaki, 1961; Vacher, 1973) and of catenary growth (Garrett and Gould, 1984) to unravel the sequence of deposition exposed on the island (Fig. 2). The former principle states that, on a prograding shoreline, deposits become younger seaward. In contrast, the latter one asserts that catenary ridges are younger than their anchoring headlands. Carew and Mylroie (1995a) have discussed the limitations of this method pertaining to the varying height of sea level at times of deposition and to the composite nature of some ridges. It follows that the morphostratigraphic approach using DEMs, topographic maps or air photographs can be helpful to get a first approximation of depositional sequences, but it has to be complemented by detailed field, sedimentological and petrographic studies.

3.2. Fieldwork and sample collection

This investigation included petrographic, sedimentological, paleontological, and geomorphological examination of exposed rock bodies. Stratigraphic sections (generally low sea cliffs, platforms, and roadcuts) were measured and described in details. Physical and biogenic sedimentary structures, biogenic constituents and stratigraphic relationships between units were recorded photographically. Hand sampling was made at closely spaced intervals in each unit or subunit. All samples were later impregnated with blue-stained epoxy resin, thin sectioned, and examined with a light-transmitted microscope to determine the early diagenetic history, and identify the possible imprint of pedogenic processes. We paid particular attention to indicators of ancient RSLs such as in-growth coral specimens, coralline algae caps, fenestral porosity and fossil beach deposits (Section 3.3.; Rovere et al., 2016; Dutton et al., 2022). These indicators (see Section 5.3) are located on or within 10 m of the shoreline, and their elevation was measured with a metered tape relatively to the contemporaneous sea level. According to Rovere et al. (2016), this procedure implies a vertical error of *ca.* ± 10 % of the elevation measurement. Accounting for an additional tidal range of ± 0.5 m (Dyer et al., 2021), a conservative vertical uncertainty of ± 0.6 m was adopted.

3.3. Indicators of past sea level

Only the indicators of past sea level that have been identified and used in this study are presented below. A detailed summary of other markers can be found in Rovere et al. (2016) and Dutton et al. (2022). We applied the concepts and the equations presented in Rovere et al. (2016) to reconstruct the paleo RSL: namely, the indicative range (IR) which is the elevation range over which an indicator may form, and the reference water level (RWL) which is the mid-point of this range.

3.3.1. Corals

Single coral species can only be considered as marine-limiting



Fig. 2. Strand plain at Prime Cay, Exumas, illustrating the morphostratigraphic mapping method used in this study. The beach ridges of Holocene age prograded seawards and post-date the Pleistocene headlands on which they are anchored. The age succession is as follows: 1 > 2>3 > 4. Image from Google Earth.

indicators of past sea level (Dutton et al., 2022). Their depth range is generally important (e.g. between −1.5 and −13 m for *Pseudodiploria* sp.; Hibbert et al., 2016) which introduces a considerable uncertainty in the estimation of paleo RSL positions. However, coral specimens, when unaltered, have the great advantage to be precisely datable with various dating methods (^{14}C , U-series).

3.3.2. Red-algal caps

The crest and flat portion of high-energy reefs are commonly encrusted by coralline algae, including both branching and crustose forms, that provide more precise constraints on sea-level position than the corals themselves. In such a setting, these organisms typically occur within the uppermost subtidal to intertidal zone at a depth of around -0.4 ± 0.2 m (Hattin and Warren, 1989). Unfortunately, calcareous red algae are not a suitable material for age determination with the U-series method (Linge et al., 2008).

3.3.3. Sandy carbonate coastal deposits

The progradation of sandy carbonate shorelines generates a vertical succession of physical sedimentary structures comprising (from base to top) small-scale trough cross-beds, low-angle seaward-dipping cross-beds with keystone vugs, and high-angle, landward-dipping foresets, corresponding respectively to sediment deposition in subtidal, intertidal, and supratidal settings (Davaud and Strasser, 1984). The beach to dune transition corresponds to the level of the swash limit of constructive waves, and is therefore considered as a direct indicator of mean sea level (Tamura, 2012; Dutton et al., 2022). Fossil sandy carbonate shoreline deposits can further be coarsely dated with several methods (U-Th dating, AAR dating), and are thus a prime indicator to pinpoint ancient sea levels (Dutton et al., 2022).

3.4. Geochronological methods

3.4.1. ^{14}C dating

Samples assumed to be of Holocene age were forwarded to the Keck Carbon Cycle AMS facility at the Earth System Science Department of

the University of California, Irvine. Approximatively 1 g of material was analyzed following the low-precision ^{14}C dating method (Table 4) developed by Bush et al. (2013). Radiocarbon concentrations are given as fractions of the Modern standard, D^{14}C , and conventional radiocarbon age, following the conventions of Stuiver and Polach (1977). Sample preparation backgrounds have been subtracted, based on measurements of ^{14}C -free marble. All results have been corrected for isotopic fractionation according to the conventions of Stuiver and Polach (1977). Comparison between the low-precision and high-precision methods showed an average deviation of 1.8 % of the obtained ages for samples younger than 10 ka BP.

3.4.2. Sr-isotope dating

Samples presumed to be of early or middle Pleistocene age, and devoid of pedogenic textures, were measured with a Thermo Neptune PLUS Multi-Collector ICPMS in static mode at the University of Geneva after separation and cleaning procedures were carried out (Horwitz et al., 1992). The $^{87}\text{Sr}/^{86}\text{Sr}$ ratio of 8.375209 served as a metric to monitor instrumental mass fractionation during the analysis. Concurrently, interferences at masses 84 (^{84}Kr), 86 (^{86}Kr), and 87 (^{87}Rb) were rectified in-run by tracking ^{83}Kr and ^{85}Rb . The external reproducibility (2σ) of the SRM987 standard was 27 ppm, and all measured ratios were normalized to the standard given value ($^{87}\text{Sr}/^{86}\text{Sr} = 0.710248$; McArthur et al., 2001). Numerical ages were then obtained by comparison with the Sr-isotope evolution of global seawater for the Neogene reported as the look-up table Version 4:08/04 (Howarth and McArthur, 1997; McArthur et al., 2001).

3.4.3. Amino-acid racemization (AAR) dating

The outer layer (ca. 10–15 cm) of whole-rock samples was removed to avoid any potential contamination from surface processes. All samples were sent for analysis to the Amino Acid Geochronology Laboratory of the Northern Arizona University where they were powdered (250 μm –1 mm) and leached in dilute hydrochloric acid (Hearty and Kaufman, 2000). The amino-acid content was then measured by reverse phase high-performance liquid chromatography (Kaufman and Manley, 1998),

and the alloisoleucine/isoleucine (A/I) ratios were calculated from the measured D/L ratios of valine (Whitacre et al., 2017). The A/I ratio amounts to zero in modern sediments, and increases to an equilibrium value of 1.3 for infinite-age rocks (Hearty and Kaufman, 2000, 2009).

3.4.4. U-series dating

Fragments of the dense skeletal wall of pristine corals as well as

oolite samples were sent to the Radiochronology Laboratory of GEOTOP in Montreal, Canada. Most samples were X-rayed to quantify the amount of diagenetic calcite. Unfortunately, the laboratory did not provide us with the calcite content for all samples. In that case, determination of the alteration grade was conducted by petrographic investigations. Approximately 1 g of material was crushed into a fine powder and sent for analysis using a multi-collector inductively coupled plasma mass



Fig. 3. Geological map of Long Island draped on the shaded DEM to show landform morphology and spatial arrangement of the allostratigraphic units. The locations of interest mentioned in the text are also displayed.

spectrometer (MC-ICP-MS). For U and Th extraction, all samples underwent total sample dissolution using a mixture of HCl, HNO₃, and HF. The chemical extraction procedures for U and Th involved two stages. In the first stage, a Biorad AG 1 × 8™ resin was utilized with 6N HCl and H₂O to separate U and Th. In the second stage, U was purified using a U/Teva™ resin with 0.02N HNO₃, while Th was purified using an AG 1 × 8™ resin with 6N HCl (Carter et al., 1999). To determine chemical and ionization efficiencies, a combined ²³³U–²³⁶U–²²⁹Th spike was employed.

All reported U-Th ages are single-sample ages and isotope evolution diagrams (²³⁴U/²³⁸U vs. ²³⁰Th/²³⁸U) were used to evaluate detrital Th contributions and initial ²³⁴U/²³⁸U signatures. We applied the flexible screening protocol recommended by Chutcharavan and Dutton (2021) to assess the reliability of our dating results on coral samples: (1) the amount of diagenetic calcite must be less than 5 %; (2) the ²³⁸U concentration value must range between 2.0 and 4.0 ppm; (3) the ²³²Th concentration value must be less than 12 ppb; (4) the initial ²³⁴U/²³⁸U activity ratio ($\delta^{234}\text{U}_i$) must be comprised between 140 and 152 ‰. Ages obtained from samples that meet all the criteria listed above are considered as “reliable”. Ages from samples that meet all but one criterion are deemed as “possibly reliable”, as long as the faulty value is close to the accepted limit (e.g., $\delta^{234}\text{U}_i = 154$ ‰). The amount of calcite cement was not considered in the case of oolite samples as it generally carries little or no U (Muhs et al., 2020).

4. Results

We have identified eight distinct rock bodies on Long Island that can best be defined as allostratigraphic units because they represent mappable, superposed or contiguous, discontinuity-bounded deposits of similar or heterogeneous lithology.

(North American Commission on Stratigraphic Nomenclature, 2021). Their main characteristics are briefly described in the following sections, and their spatial distribution is illustrated in Figs. 3 and 4.

4.1. Dunmore Cave unit

This unit is well exposed at Dunmore Cave, Hamilton Cave, and Petty's Quarry. Smaller outcrops occur at Great Harbour, Indian Head Point, and Bain's Bluff. The GPS coordinates of these localities can be found in Table S1. SE of Clarence Town, the Dunmore Cave unit forms a series of NW-SE trending hillocks parallel to both the shoreline and the

platform margin. To the west of this locality, it represents the core of the ca. 15-km long, NW-SE trending ridge stretching from Victoria Village to Buckley Settlement (Fig. 3). Steep foresets with a landward dip can be observed at all exposures. The Dunmore Cave unit is made of fine-grained, well-sorted bioclastic grainstones (Fig. 5A). Bioclasts are partly dissolved, micritized or recrystallized. They mainly include porcelaneous benthic foraminifers, echinoid debris, spar-filled micritic envelopes as well as red-algae fragments. Peloids, ooids, and lumps are scarce. Cement consists of fine low-Mg calcite (LMC) spar forming menisci between grains, circumgranular rims, and filling pore spaces. Porosity is diverse: intergranular, intragranular, and moldic. The lower boundary of the unit is never visible, whereas the upper one, exposed at Petty's Quarry (Fig. 6A), is marked by a brown micritic crust. ⁸⁷Sr/⁸⁶Sr ratios measured at Hamilton cave, Dunmore Cave, and Petty's Quarry average at 0.709157 ± 0.000004 (n = 3; Table 1).

The overall morphology, fine-grain size, landward-dipping foresets, and the occurrence of meniscus cement attest of an eolian origin for these deposits. Sr-dating results indicate an age between ca. 700 and ca. 450 ka BP (Howarth and McArthur, 1997; McArthur et al., 2001, 2020), which spans the time interval between MIS 17 and MIS 12 (Lisiecki and Raymo, 2005). The Dunmore Cave unit can thus be safely placed in the middle Pleistocene, which is further confirmed by its morphostratigraphic position and fairly high degree of diagenetic alteration.

4.2. Petty's Quarry unit

This unit is best exposed at Petty's Quarry (Fig. 6A). Smaller outcrops can be examined at Miller's Bay, Thompson Bay, and Neptune Cay on the lee side of Long Island, and at Dean's Bay on the Ocean side (Table S1). The Petty's Quarry unit forms part of the large NW-SE trending ridge stretching between Victoria Village and Buckley that may reach up to 30 m in elevation. The exposures on the lee side of the island are represented by small, low headlands or cays. Large-scale, landward-dipping foresets occur at most outcrops and fenestrae-rich, planar beds inclined towards the ocean can also be observed at Petty's Quarry at the elevation of ca. 20 m. The Petty's Quarry unit is a well-lithified, well-sorted oopelsparite containing few bioclasts (Fig. 5B). Ooids are commonly wholly or partly leached or calcitized whilst peloids also show evidence of recrystallization. Cement is made of LMC equant spar forming menisci and filling pores. Early rim cement can be observed in a few samples. Porosity is varied: intergranular, moldic, micromoldic, vuggy, and fenestral in some samples. The boundary with

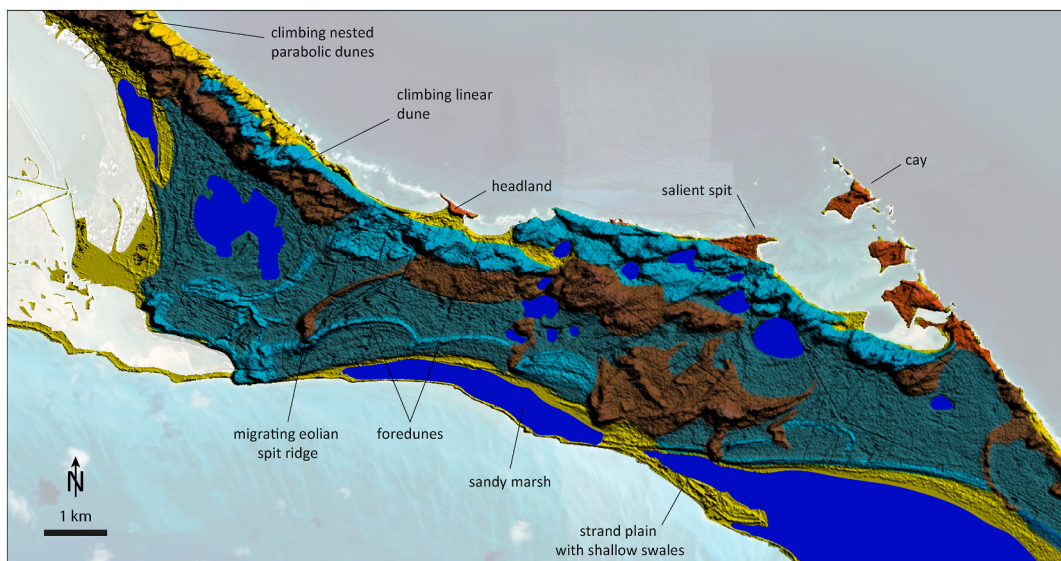


Fig. 4. Detailed map of the central part of Long Island showing the complex arrangement of the identified geological units and their main geomorphological expressions.

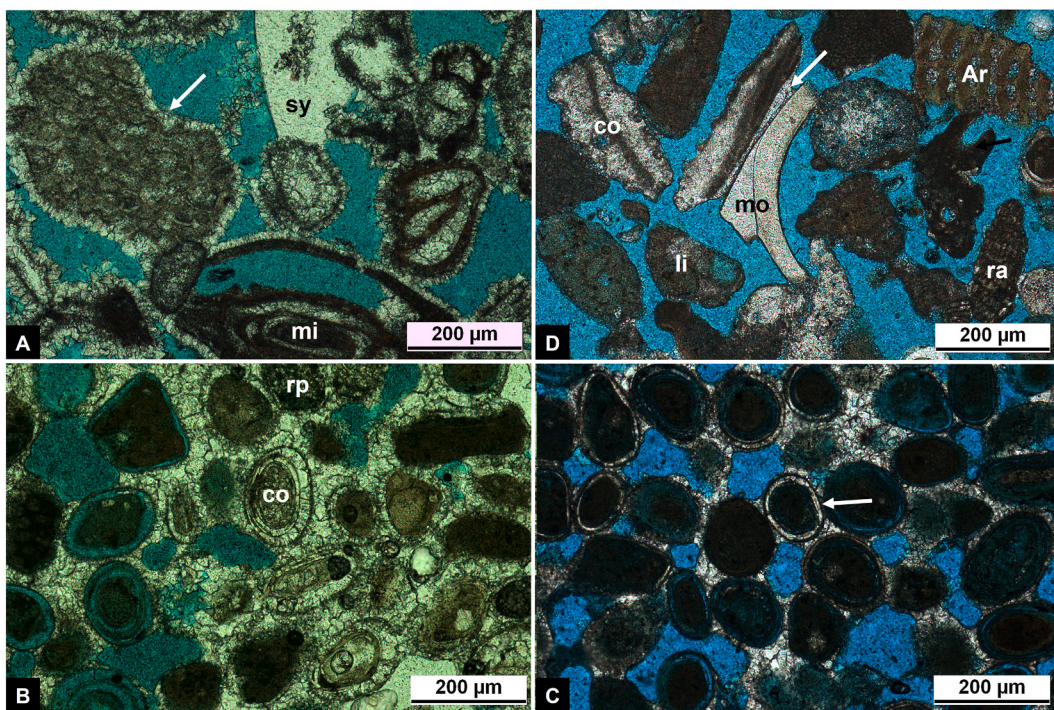


Fig. 5. **A.** Microfacies of sample LI 11 collected from the Dunmore Cave exposure. Altered biosparite. Most bioclasts are recrystallized or represented by a spar-filled micritic envelope. Note LMC rim cement (arrow) around grains, high porosity (especially intergranular), and the lack of recent cement; mi = miliolid; sy = syntaxial cement around echinoid fragment. **B.** Microfacies of sample LI 26 collected at Petty's Quarry (black dot in Fig. 6A). Altered oopelssparite. Grains, most of which are recrystallized and/or leached, mainly include tangential ooids and peloids; co = calcitized ooid, rp = recrystallized peloid. **C.** Microfacies of sample LV 26 collected from the ridge located to the north of Turnbull Settlement. Oopelssparite. Grains essentially comprise thinly and thickly coated ooids, some of which showing a partially calcitized cortex (white arrow). Note lesser diagenetic alteration than on Fig. 5B. **D.** Microfacies of sample LI 16 collected from the South Point exposure (Fig. 9B). Ar = *Archaias* sp., co = coral, ra = red algae, mo = mollusk, li = opelmicrite lithoclast. Arrow points to rare LMC meniscus cement. Note important intergranular porosity and lesser degree of diagenetic alteration than on Fig. 5A. (For interpretation of the references to colour in this figure legend, the reader is referred to the Web version of this article.)

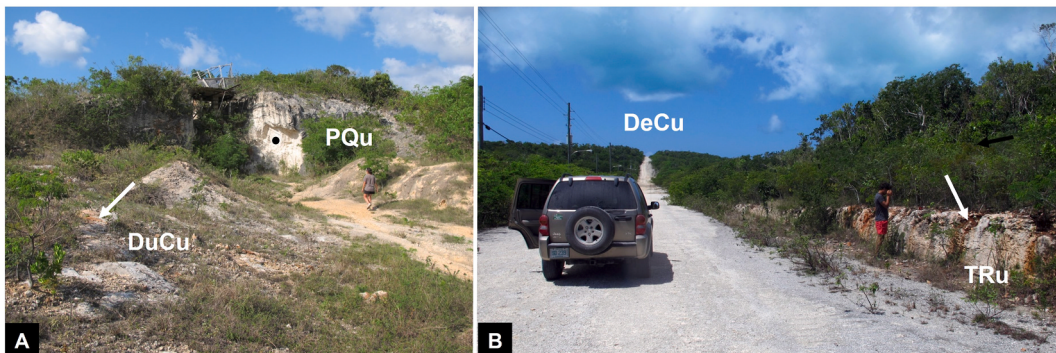


Fig. 6. **A.** Partial view of the Petty's Quarry exposure showing the superimposition of the Dunmore Cave unit (DuCu, skeletal) and of the Petty's Quarry unit (PQu, oolitic). White arrow points to the partially preserved brown micritic crust capping the lower unit. Black dot indicates the locus where sample LI 26 was collected. Person for scale is 1.58 m tall. **B.** NE-SW trending roadcut located to the South of Stevens Settlement showing the upper boundary of the Turnbull Ridge unit (TRu). The overlying Deadman's Cay unit (DeCu) is visible in the background. Note paleosol-fill pits in the upper part of the lower unit (white arrow). Person for scale is 1.83 m tall. (For interpretation of the references to colour in this figure legend, the reader is referred to the Web version of this article.)

Table 1
Sr-isotope dating results from the Dunmore Cave unit.

Sample #	Outcrop	$^{87}\text{Sr}/^{86}\text{Sr}$	STD	$^{87}\text{Sr}/^{86}\text{Sr}$	STD	Age range (ka BP)	
		measured		normalized		min.	max.
LI 10	Hamilton Cave	0.709181	0.000003	0.709153	0.000007	461	879
LI 11	Dunmore Cave	0.709184	0.000001	0.709156	0.000002	512	690
LI 25	Petty's Quarry	0.709189	0.000002	0.709161	0.000003	342	632

STD = standard deviation.

the underlying Dunmore Cave unit is visible at Petty's Quarry (Fig. 6A), but the upper boundary always corresponds to the island surface. A/I ratios measured on samples from Petty's Quarry and Dean's Bay return an average value of 0.652 ± 0.159 ($n = 2$; Table 2).

The overall morphology and the occurrence of large-scale, landward-dipping foresets attest of a predominantly eolian depositional setting for this unit. However, at Petty's Quarry, the fenestrae-rich, planar beds could also represent an elevated beach facies. The Petty's Quarry unit can be placed in the middle Pleistocene because of its morphostratigraphic position and high degree of diagenetic alteration. This attribution is further supported by the results of AAR dating. The latter correspond to Aminozone H of Hearty and Kaufmann (2000, 2009), which is correlated with MIS 11 (ca. 430 to 365 ka BP; Lisiecki and Raymo, 2005).

4.3. Turnbull Ridge unit

This unit can be observed along Queen's Highway to the east of Stevens Settlement, at Burrows Harbour in the southern part of Long Island, and possibly along the Ocean coast to the east of Gray's Settlement (Table S1). It is essentially represented in a SW-NE trending, ca. 1.5 km-long, low-elevation ridge displaying rare high-angle cross-bedding and rhizoliths. The Turnbull Ridge unit consists of a well-sorted

peloobiosparite with most grains being somehow altered (recrystallization, micritisation) and partly leached, thus precluding precise identification. Allochems are represented by algal peloids (after *Halimeda*), bahamite peloids (after ooids and bioclasts), pelletoids, cortoids, aggregates, and both tangential and radial ooids. Cement is made of fine LMC spar forming menisci, partial rims, and filling pores. Porosity is intergranular and (micro)moldic. The lower boundary has never been observed. The upper boundary is visible along the dirt road between Turnbull and Stevens settlements where the Turnbull Ridge unit is capped by the Deadman's Cay unit (see section 4.5.). Both units are separated by a deep-red paleosol at this location (Fig. 6B). Only one A/I ratio amounting to 0.454 ± 0.001 was obtained from the exposure along Queen's Highway near Turnbull Settlement (Table 2).

This unit can be interpreted as an eolianite based on the overall shape of the deposits, and the occurrence of high-angle cross-bedding, rhizoliths and LMC meniscus cement. The obtained A/I ratio corresponds to the limit between Aminozone E and F/G (Hearty and Kaufman, 2000, 2009), which are correlated with MIS 5e and MIS 7 to 9, respectively. Considering its petrographic composition, its fairly high degree of diagenetic alteration, and its position below a *terra-rossa* paleosol capped by a well-identified unit of late Pleistocene age, we can assign the Turnbull Ridge unit to the middle Pleistocene, likely to MIS 7 or 9 (337-191 ka BP; Lisiecki and Raymo, 2005).

4.4. Little Harbour unit

This unit is best exposed at Little Harbour, to the East of Roses, and on the eastern side of Deans' Bay (Table S1). At the type section, the Little Harbour unit forms one ca. 2 km-long, low platform showing an undulating topography (Fig. 7A). The ‘highs’ represent elongated, dome-shaped, m-scale bioherms trending towards the NE, and reaching a maximum elevation of $+2.5 \pm 0.5$ m above MSL. The intervening lows, which are generally sand-filled, range from a few m to a few 10s of m in width. The core of the bioherms, only visible on eroded build-ups and at low tide, is made of coral framestone/rudstone mostly comprising well-preserved (i.e., still aragonitic), fragile coral species such as *Acropora cervicornis*, *Porites porites* and *Agaricia agaricites* (Fig. 7B). These corals are capped by a 20 to 30 cm-thick bindstone layer composed of crustose and branching coralline algae, vermetid gastropods (*Dendropoma* sp.), serpulids, encrusting foraminifers (*Homotrema rubrum*, *Nubecularia* sp., *Rupertina* sp.) and microbialites (Fig. 7B). Locally, this bindstone layer supports an upper coral framestone made of *Pseudodiploria* sp. and *P. clivosa* (Fig. 7C). The surface separating the bindstone from these coral colonies is sharp and microbored, but does not show evidence of significant erosion and/or pedogenesis (Fig. 7D). At Dean's Bay, the unit comprises one m-scale mound exclusively composed of *A. cervicornis* framestone encrusted by red algae (Fig. 8A), and locally surrounded by a floatstone containing fragments of the same coral species. The lower boundary of the Little Harbour unit is not observable as it always occurs below sea level. The upper boundary, which can be seen at both locations, corresponds to a conformable surface with the overlying Deadman's Cay unit (Fig. 8A and 9A; see Section 4.5.). At Little Harbour, the bioherms are locally capped by the Dean's Bay unit. In this case, the upper boundary is a karstic surface (Fig. 7C and 8B; see Section 4.6.). The coral core of the bioherms exposed at Little Harbour yielded one reliable U-Th age of 124.6 ± 1.6 ka BP, and two possibly reliable ages that average at 128.8 ± 9.5 ka BP (Table 3). The colonies above the bindstone capping the coral core gave possibly reliable ages that average at 119.6 ± 2.4 ka BP ($n = 3$; Table 3). *A. cervicornis* samples from Dean's Bay were dated at 122.2 ± 0.2 ka BP based on one reliable and one possibly reliable age (Table 3).

At the type section, the Little Harbour unit can be interpreted as the spur and groove system of a fringing reef, whilst at Dean's Bay it corresponds to a lagoonal patch reef. The U-Th dating results allow to confidently correlate this unit with the last interglacial period (MIS 5e; 128-116 ka BP, Stirling et al., 1998).

Table 2
Amino-acid racemization data. A/I = alloisoleucine/soleucine ratio.

Lab #	Field #	Exposure	Unit	A/I	
10981	LI 26	Petty's Quarry	Petty's Quarry	0.764	± 0.029
10976	LI 35	Dean's Bay	Petty's Quarry	0.539	± 0.006
		average		0.652	± 0.159
13694	LV 14	Queens' Hwy	Turnbull Ridge	0.454	± 0.001
10982	LI 42	Little Harbour	Deadman's Cay	0.555	± 0.022
13704	LI 63	Little Harbour	Deadman's Cay	0.527	± 0.003
17024	LI 133	Miller's	Deadman's Cay	0.419	± 0.002
13696	LV 19	Queens Hwy	Deadman's Cay	0.388	± 0.004
10979	LI 13	South Point	Deadman's Cay	0.381	± 0.008
13698	LV 26	Turnbull	Deadman's Cay	0.380	± 0.004
17019	LI 107	Old Gray's	Deadman's Cay	0.340	± 0.006
13695	LV 17	Queens Hwy	Deadman's Cay	0.338	± 0.001
13687	LV 1	Scrub Hill	Deadman's Cay	0.333	± 0.006
13688	LV 2	Scrub Hill	Deadman's Cay	0.330	± 0.002
17018	LI 106	Dean's Bay	Deadman's Cay	0.297	± 0.031
13706	LI 71	E of Roses	Deadman's Cay	0.294	± 0.001
10975	LI 22	Buckley	Deadman's Cay	0.276	± 0.016
13699	LI 45	Buckley	Deadman's Cay	0.265	± 0.000
13691	LV 7	Dean's Bay	Deadman's Cay	0.263	± 0.013
13697	LV 25	Turnbull	Deadman's Cay	0.208	± 0.013
		average		0.350	± 0.095
10977	LI 33	Little Harbour	Deans' Bay	0.399	± 0.006
17020	LI 109	Burrows Harbour	Deans' Bay	0.382	± 0.019
17022	LI 113	Clem Cay	Deans' Bay	0.363	± 0.004
17025	LI 135	Dean's Bay	Deans' Bay	0.359	± 0.003
13690	LV 4	Dean's Bay	Deans' Bay	0.343	± 0.019
13703	LI 61	Little Harbour	Deans' Bay	0.333	± 0.010
10980	LI 16	South Point	Deans' Bay	0.339	± 0.037
17023	LI 124	Deadman's Cay	Deans' Bay	0.300	± 0.003
13702	LI 53	Little Harbour	Deans' Bay	0.286	± 0.004
10978	LI 8	Clem Cay	Deans' Bay	0.278	± 0.029
13701	LI 52	Buckley	Deans' Bay	0.258	± 0.013
13700	LI 47	Buckley	Deans' Bay	0.254	± 0.008
13693	LV 12	Clarence Town	Deans' Bay	0.246	± 0.004
13705	LI 65	Roses	Deans' Bay	0.246	± 0.007
10974	LI 24	Buckley	Deans' Bay	0.243	± 0.022
13692	LV 11	Clarence Town	Deans' Bay	0.213	± 0.015
		average		0.303	± 0.056
17014	LI 127	Gray's	Buckley Settl.	0.134	± 0.001
17015	LI 131	Miller's	Buckley Settl.	0.122	± 0.000
17016	LI 134	Millerton	Buckley Settl.	0.101	± 0.004
17017	LI 136	North End	Buckley Settl.	0.120	± 0.008
13689	LV 3	Scrub Hill	Buckley Settl.	0.110	± 0.004
		average		0.117	± 0.020

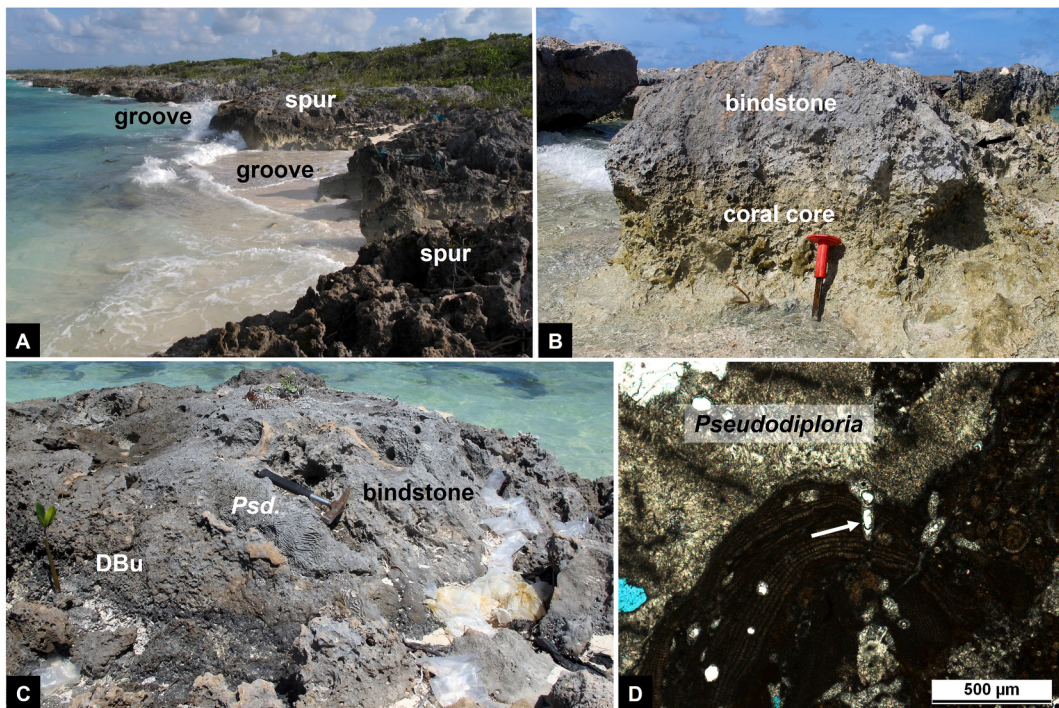


Fig. 7. A. Northern part of the Little Harbour exposure showing the succession of highs and lows interpreted as the spur and groove system of a shallow forereef zone. The spur in the upper part of the photo is 1.5 m high. B. Partly eroded bioherm revealing its internal structure which comprises one core of coral framestone/rudstone capped by an algal-foraminiferal bindstone; chisel for scale is 30 cm long. C. Partial view of the upper portion of a bioherm showing one colony of *Pseudodiploria clivosa* (*Psd.*) encrusting the underlying/adjacent bindstone layer, and capped itself by the skeletal eolianite of the Dean's Bay unit (DBu); hammer for scale is 35 cm long. D. Microscopic view of the boundary between one colony of *P. clivosa* and the underlying algal-foraminiferal bindstone. The boundary is sharp, but not erosional save for some microborings (white arrow), and the bindstone does not show any evidence of pedogenic alteration.

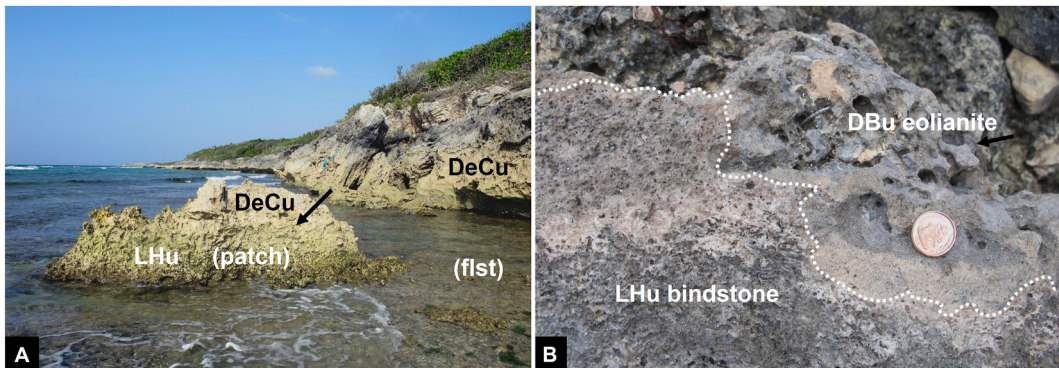


Fig. 8. A. Partial view of the exposure on the east side of Dean's Bay showing the boundary between the Little Harbour unit (LHu) and the overlying Deadman's Cay unit (DeCu). Black arrow points to the boundary. The former unit is represented by a lagoonal patch reef (patch) surrounded coral floatstone (flst), the latter by a rhizolith-rich eolianite. B. Close-up view of the karstic surface separating the Little Harbour unit (LHu) from the overlying Dean's Bay unit (DBu) at Little Harbour.

4.5. Deadman's Cay unit

This unit is by far the most extensive rock body on Long Island. Key exposures include (from North to South) those at Millers, Old Gray, Deadman's Cay, Buckley, Scrub Hill, Dean's Bay, Turnbull, Great Harbour, Roses, and South Point (Table S1). The Deadman's Cay unit comprises a variety of landforms including high-elevation, arcuate and linear ridges parallel to the coast, low-lying parabolic dunes, and strand plains with shallow swales. It further displays numerous, well-preserved, large- and small-scale sedimentary structures. High-angle, landward-dipping foresets, subcritically translatent stratification, grainfall and grainflow laminae, and rhizoliths predominate in the higher reaches of the unit, whereas low-angle cross beds with a seaward dip and herring-bone cross bedding can be observed at low elevations.

The uppermost elevation of the low-angle cross beds occurs at $+2.5 \pm 0.5$ m above MSL to the east of Deadman's Cay. The Deadman's Cay unit comprises moderately to well-sorted, light gray to white, predominantly oolitic-peloidal grainstones with a variable proportion of bioclasts and aggregates. Ooid cortices are often leached and can also be partly calcitized, whereas nuclei are always well preserved (Fig. 5C). Porosity is high, intergranular and micromoldic. Cement is made of fine LMC crystals forming menisci between grains, and locally filling pore spaces. The lower boundary is exposed along the road between Turnbull and Stevens settlements where a deep-red paleosol can be observed between the Deadman's Cay unit and the underlying Turnbull Ridge unit (Fig. 6B). At Dean's Bay (Fig. 8A) and at Little Harbour (Fig. 9A), the unit conformably overlies the coral-rich Little Harbour unit, but at many locations (e.g., along the Ocean coast to the west of Clarence Town), the

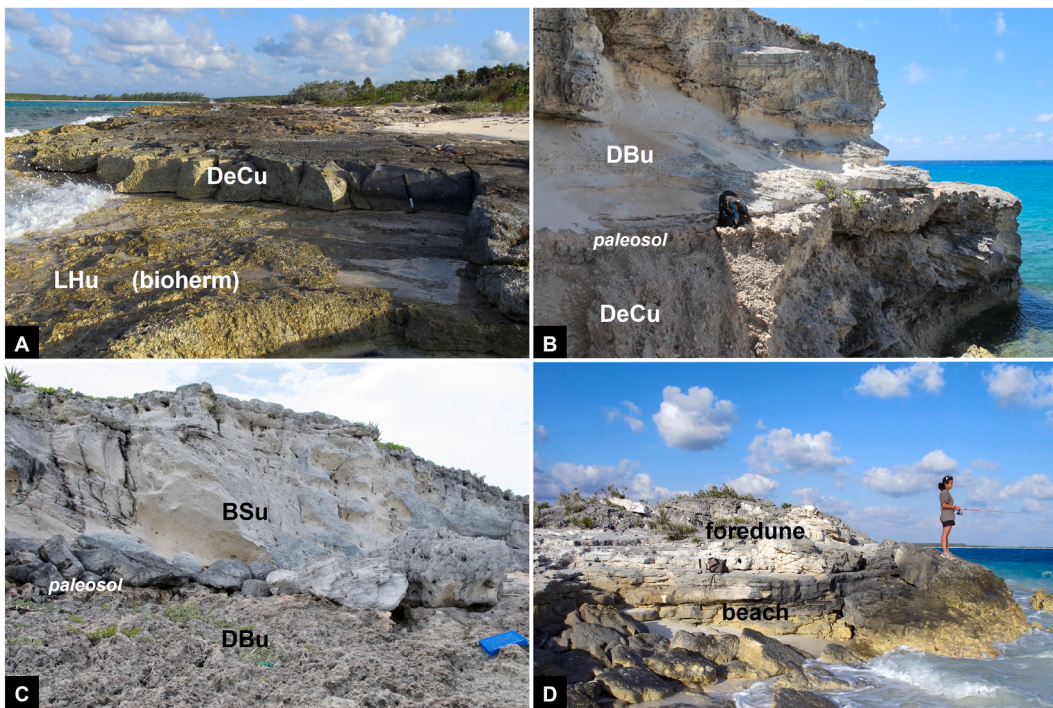


Fig. 9. **A.** Partial view of the Little Harbour exposure showing the conformable limit between the Little Harbour unit (LHu), below, and the Deadman's Cay unit (DeCu), above. The former unit is represented by a corallgal framestone/bindstone, the latter one by oolitic-peloidal deposits. Hammer for scale is 35 cm long. **B.** Upper boundary of the Deadman's Cay unit (DeCu) at South Point. The unit is separated from the overlying Dean's Bay unit (DBu) by a 30-cm thick paleosol. Bag for scale is 50 cm high. **C.** Northern part of the Buckley exposure showing the vertical stacking of the Dean's Bay (DBu) and Buckley Settlement (BSu) units. The boundary corresponds to a paleosol. The crate on the right-hand side for scale is 50 cm long. **D.** Partial view of the Stevens Salina unit exposure at Turnbull. Person for scale is 1.58 m tall. Note that the beach facies is congruent with MSL.

lower boundary occurs below sea level. At several sites (e.g., South Point, Roses, Buckley), the upper boundary of the Deadman's Cay unit corresponds to a karstic surface or a paleosol that separates it from the overlying Dean's Bay unit (Fig. 9B; see Section 4.6.), but in most places, this limit is just a cm-thin calcrete at the atmosphere-lithosphere boundary. Sixteen A/I ratios averaging at 0.350 ± 0.095 were obtained from this unit (Table 2). One semi-reliable U-Th age of 114.8 ± 2.2 ka BP was also measured on one oolite sample collected from the base of the unit at Little Harbour (Fig. 9A; Table 3).

Relying of the observed sedimentary structures, the Deadman's Cay unit can be interpreted for the large part as an eolian deposit, but it can locally include intertidal (e.g., along the Ocean coast to the west of Clarence Town) and subtidal sediments (e.g., at Millerton) in its lower reaches. The mean A/I ratio corresponds to the uppermost portion of Aminozone E (Hearty and Kaufman, 2000, 2009), which is correlated with MIS 5e. Considering the overall position of the unit in the stratigraphic record, the local occurrence of marine facies above MSL and the measured U-Th age, we assign it to the late part of MIS 5e (128–116 ka BP, Stirling et al., 1998).

4.6. Dean's Bay unit

This unit occurs along the eastern coast of Long Island, particularly at Deadman's Cay, Buckley, Dean's Bay, Bonne Cord, Clem Cay, Little Harbour, Burrow's Harbour, to the East of Roses and at South End (Table S1). It generally forms low-elevation (up to 10 m) coastal and offshore ridges, as well as headlands that serve as anchors for modern pocket beaches. These landforms display a large variety of cross stratifications dipping at various angles, and extensive penetrative (up to 3 m) networks of rhizoliths towards their top. The Dean's Bay unit consists of light tan, weakly indurated, bioclastic grainstones (Fig. 5D). The most frequent bioclasts include porcelaneous benthic foraminifera (miliolids,

soritids), *Homotrema rubrum*, mollusk, red algae, *Halimeda* sp. and dasyclad algae. Ooids, lumps and oolite lithoclasts are common in some landforms, likely corresponding to the lower reaches of the unit. The scarce cement consists of fine LMC equant spar generally forming menisci between grains. Intergranular porosity is high, intragranular porosity is common. The lower boundary of the unit often occurs below sea level. At several places (Deadman's Cay, Buckley, Roses, Little Harbour, South Point), however, it can be observed, and corresponds to a karstic surface or a paleosol capping the underlying Little Harbour or Deadman's Cay units, as is the case at South Point (Fig. 9B). The upper boundary is visible at Buckley where the Dean's Bay unit is separated from the overlying Buckley Settlement unit (see Section 4.7.) by a paleosol (Fig. 9C). Nonetheless, at most sites, the upper surface is marked by a cm-thin calcrete at the atmosphere-lithosphere boundary. Sixteen A/I ratios averaging at 0.303 ± 0.056 were retrieved from this unit (Table 2).

The Dean's Bay unit can be confidently identified as an eolianite based on the overall shape of the deposits, and the occurrence of high-angle cross-bedding, rhizoliths and LMC meniscus cement. The mean value of the obtained A/I ratios corresponds to Aminozone C (Hearty and Kaufman, 2000, 2009), which is correlated with MIS 5a (88–74 ka BP; Lisiecki and Raymo, 2005). This attribution is further confirmed by the position of this unit between deposits of LIG age below and Holocene age above.

4.7. Buckley Settlement unit

This unit is particularly well exposed along the northern and eastern shoreline of Long Island, notably (from North to South) at Columbus Monument, Millerton, McKann's, Gray's, Buckley, and Scrub Hill (Table S1). It usually forms narrow coastal ridges, up to 5 m high, consisting of juxtaposed dome-shaped dunes. These ridges commonly

Table 3
U-series dating results from the Little Harbour and the Deadman's Cay units.

Field #	Sample type	Setting	Loc.	DP	% calc.	238U (ppm)	232Th (ppb)	234U/238U	230Th/238U	230Th/234U	8234Ui (%)	Age (ka)	Rel.
LI 39	<i>Ps. off. clivosa</i>	in growth	LH	2	4	2,930 ± 0.033	0.190 ± 0.002	1.119 ± 0.014	0.678 ± 0.006	0.759 ± 0.009	167 ± 18	119.7 ± 3.9	PR
LI 43	<i>Ps. sp.</i>	in situ	LH	2	minor	3,317 ± 0.021	9,080 ± 0.065	1.111 ± 0.009	0.685 ± 0.005	0.761 ± 0.005	157 ± 12	121.9 ± 2.5	PR
LI 62	<i>Ps. strigosa</i>	in growth	LH	2	0	2,505 ± 0.015	0.102 ± 0.001	1.114 ± 0.008	0.670 ± 0.004	0.746 ± 0.005	158 ± 10	117.2 ± 2.2	PR
LI 77	<i>Po. asteroides</i>	in situ	LH	1	3	2,619 ± 0.007	0.257 ± 0.001	1.102 ± 0.005	0.692 ± 0.003	0.763 ± 0.003	145 ± 7	124.6 ± 1.6	R
LI 78	<i>Obicella</i> sp.	in situ	LH	1	minor	2,464 ± 0.017	6,596 ± 0.060	1.116 ± 0.011	0.725 ± 0.007	0.809 ± 0.006	170 ± 15	135.5 ± 3.6	PR
LI 130	<i>Ac. cervicornis</i>	in growth	LH	1	minor	2,983 ± 0.019	3,167 ± 0.022	1.114 ± 0.008	0.684 ± 0.005	0.762 ± 0.006	161 ± 11	121.5 ± 2.5	PR
LI 104	<i>Ps. strigosa</i>	in growth	DB	2	minor	2,985 ± 0.020	0.001 ± 0.002	1.113 ± 0.008	0.675 ± 0.005	0.751 ± 0.006	158 ± 11	119.0 ± 2.0	R
LI 103	<i>Ac. cervicornis</i>	in growth	DB	1	minor	3,405 ± 0.025	0.093 ± 0.001	1.127 ± 0.012	0.687 ± 0.006	0.774 ± 0.007	179 ± 15	122.3 ± 3.2	PR
LV 31	<i>Ac. cervicornis</i>	in growth	DB	1	0	3,388 ± 0.009	0.295 ± 0.001	1.106 ± 0.005	0.685 ± 0.003	0.757 ± 0.003	150 ± 7	122.0 ± 1.5	R
LI 42	oopelsparite	intertidal	LH	high	2,517 ± 0.017	7,370 ± 0.053	1.121 ± 0.009	0.663 ± 0.004	0.743 ± 0.005	167 ± 11	114.8 ± 2.2	PR	
LI 63	oopelsparite	intertidal	LH	high	2,004 ± 0.014	7,456 ± 0.070	1.168 ± 0.010	0.768 ± 0.005	0.897 ± 0.007	256 ± 13	149.9 ± 3.7	UR	
LV 7	ooobisparite	oolian	DB	high	2,499 ± 0.007	25,063 ± 0.088	1.130 ± 0.005	0.716 ± 0.003	0.809 ± 0.003	189 ± 7	132.0 ± 1.7	UR	
LI 105	ooobisparite	oolian	DB	high	1,762 ± 0.021	55,163 ± 0.345	1.171 ± 0.016	0.739 ± 0.007	0.866 ± 0.010	253 ± 21	139.0 ± 5.0	UR	

Loc. = Location; DP = Depositional Phase; calc. = calcite; LH = Little Harbour; DB = Dean's Bay; Rel. = reliability; PR = possibly reliable; R = reliable; UR = unreliable. Ps. = Pseudodiploria; Po. = Porites; Ac. = Acropora.

display well-preserved, fine-scale structures such as subcritically translatent stratification, grainfall and grainflow laminae, and large-scale foresets that generally dip below sea level. The Buckley Settlement unit consists of pristine oolitic-peloidal grainstones cemented by fairly coarse LMC equant spar forming menisci between grains and/or filling pores. The tangential ooids (both thinly and thickly coated) commonly show partially leached cortices. Porosity is thus fairly high, intergranular and micromoldic. The lower boundary can only be observed at Buckley where these oolitic-peloidal grainstones are separated from the underlying Dean's Bay unit by a paleosol (Fig. 9C), otherwise, as stated above, it occurs below MSL. The upper boundary always corresponds to the atmosphere-lithosphere boundary, and is locally marked by a mm-thin micritic crust. Low-precision ^{14}C ages and A/I ratios obtained from the Buckley Settlement unit average, respectively, at $6'282 \pm 1'324$ yBP (n = 6; Table 4) and at 0.117 ± 0.020 (n = 5; Table 2).

Based on its morphology and on the occurrence of large-scale and small-scale eolian structures, the Buckley Settlement unit can definitely be identified as an eolianite. Furthermore, its position above a paleosol capping a Pleistocene unit and the high proportion of large-scale, steeply dipping foresets show that it can, at least locally, be interpreted as advancing dunes (Rowe and Bristow, 2015) detached from their source beaches. The mean value of the obtained A/I ratios corresponds to the beginning of Aminozone A (Hearty and Kaufman, 2000, 2009), i.e. with the middle Holocene (8.2–4.2 ka BP; Walker et al., 2012), which is further confirmed by the ^{14}C data.

4.8. Stevens Salina unit

Essentially exposed on the lagoon side of the island near Turnbull, at Gordon, and at Ferguson Point (Table S1), this unit forms low-elevation ridges comprising seaward-dipping, fenestrae-rich beds at the base and large-scale, landward-dipping foresets with rhizoliths at the top (Fig. 9D). These ridges are made of well-preserved oolitic-peloidal grainstones cemented by LMC equant spar. Ooids are mostly unaltered save for some micritization and boring porosity. The calcite cement fills pores in the lower reaches of the unit, whereas it forms menisci between grains its upper part. The lower boundary of the Stevens Salina unit is not exposed on the studied outcrops. The upper one corresponds to the atmosphere-lithosphere boundary, and is devoid of a capping micritic crust. Low-precision ^{14}C ages average at $1'865 \pm 210$ yBP (n = 4; Table 4).

Based on the observed sedimentary structures and cement types, the Stevens Salina unit can be interpreted as a shallowing-upward sequence from beach to eolian deposits. The uppermost elevation of the beach facies is between 0 and $+1.0 \pm 0.5$ m above MSL. Based on the ^{14}C data, this unit can be attributed to the late Holocene (4.2 ka BP to Present; Walker et al., 2012).

5. Discussion

5.1. Comparison with previous research on the stratigraphy of the Bahamas

The stratigraphic record from Long Island does not significantly differ from those observed elsewhere in the Bahamas (Table 5). Truly, we did not recognize rock bodies older than the middle Pleistocene, as is the case in Mayaguana where lower Pleistocene and Neogene units are exposed (Kindler et al., 2011; Godefroid, 2011; Godefroid et al., 2019). We compare these records in the following sections.

5.1.1. Middle Pleistocene units

The Dunmore Cave unit. Hearty (2010) measured A/I ratios on skeletal rocks from Hamilton Cave, Petty's Quarry and Petty's Settlement that correspond to the Dunmore Cave unit, and also attributed them to the middle Pleistocene. This unit is thus an equivalent of one of the subunits of the OHF. Considering its petrographic composition,

Table 4
¹⁴C dating results.

Lab #	Field #	Exposure	Unit	14C age (yBP)	Fraction Modern	D14C (%)
15000	LI 21	Buckley	Buckley Settlement	7'990 ± 130	0.3697 ± 0.0056	-630.3 ± 5.7
15011	LV 3	Scrub Hill	Buckley Settlement	7'560 ± 80	0.3904 ± 0.0035	-609.6 ± 3.5
17014	LI 127	Gray's	Buckley Settlement	6'590 ± 120	0.4401 ± 0.0065	-559.9 ± 6.5
17015	LI 131	Miller's	Buckley Settlement	5'260 ± 130	0.5194 ± 0.0079	-480.6 ± 7.9
17016	LI 134	Millerton	Buckley Settlement	4'650 ± 100	0.5605 ± 0.0065	-439.5 ± 6.5
17017	LI 136	North End	Buckley Settlement	5'640 ± 120	0.4957 ± 0.0073	-504.3 ± 7.3
average				6'282 ± 1324		
15001	LI 28	Turnbull	Stevens Salina	2'130 ± 70	0.7667 ± 0.0064	-233.3 ± 6.4
15002	LI 29	Turnbull	Stevens Salina	1'640 ± 45	0.8155 ± 0.0045	-184.5 ± 4.5
15003	LV 20	Turnbull	Stevens Salina	1'920 ± 100	0.7876 ± 0.0096	-212.4 ± 9.6
15004	LV 23	Turnbull	Stevens Salina	1'770 ± 70	0.8027 ± 0.0068	-197.3 ± 6.9
average				1'865 ± 210		

Table 5
Comparison of stratigraphic schemes established for the Bahamas archipelago.

Ep.	MIS	Long Island (0)	Exumas (1)	West Caicos (2)	Mayaguana(3)	The Bahamas(4)	The Bahamas(5)	The Bahamas(6)	San Salvador (7)
Holocene	1	ND Stevens Salina u. Buckley Settl. u.	ND Unit 11b	Recent Long Road u.	ND Hanna Bay Mb.	Couplet VI	ND Unit VIII	Rice Bay Fm.	ND Hanna Bay Mb.
Late Pleistocene	5a	Dean's Bay u.	Unit 10	NR	NR		Unit VII		North Point Mb. NR
	5e	Deadman's Cay u. Little Harbour u. NR	Unit 9	NE Ridges u. Boat Cove u. South Reef u. Railroad Ridge u.	Big Cove Mb. Cockburn Town Mb. French Bay Mb.	Couplet V Couplet IV	Unit VI Unit V	Grotto Beach Fm.	Almgreen Cay Fm. Fernandez Bay Mb.
Middle Pleist.	7 to 15	Turnbull Ridge u. Petty's Quarry u. Dunmore Cave u.	Units 7 & 8 Unit 6	NR Star Town u.	Owl's Hole Fm.	Couplet III Couplet II	Units II & III Unit I	Owl's Hole Fm.	Cockburn Town Mb. French Bay Mb. Fortune Hill Fm. Owl's Hole Fm.

Ep. = Epochs; MIS = Marine Isotope Stages; ND = not differentiated; NR = not recognized (0) This paper; (1) [Hearty and Backstrom, 2021](#); (2) [Kerans et al., 2019](#); (3) [Godefroid, 2011](#); (4) [Hearty and Kaufman, 2000](#); (5) [Kindler and Hearty, 1997](#); (6) [Carew and Mylroie, 1989a](#); (7) [Hearty and Kindler, 1993a](#).

sedimentological attributes, diagenetic grade, and the obtained ⁸⁷Sr/⁸⁶Sr data, it can be more specifically correlated with Unit 0 of [Kindler and Hearty \(1997\)](#) and with Couplet I of [Hearty and Kaufman \(2000\)](#), both of which have been assigned to MIS 13 with caution. Similar and likely coeval units have been more recently observed on Mayaguana ([Godefroid et al., 2019](#)) and Crooked ([Godefroid and Kindler, 2016](#)).

The Petty's Quarry unit. [Hearty \(2010\)](#) measured one A/I ratio of 0.866 ± 0.007 on an oolitic rock body likely corresponding to the Petty's Quarry unit. He assigned this oolite to the middle Pleistocene, although the obtained ratio exceeds the practical limit of the whole-rock method. This unit can likewise be correlated with the OHF, and more specifically with the Unit I of [Kindler and Hearty \(1996, 1997\)](#) identified on New Providence, Eleuthera, and Great Abaco, and attributed to MIS 9–11. Unit I is mainly composed of altered oolitic eolianites, but also comprises marine facies at fairly high elevations (*ca.* 13 m above MSL; [Hearty et al., 1999](#)). The Star Town unit exposed in the southern part of West Caicos appears also to be a correlative unit, but of more variable petrographic composition ([Kerans et al., 2019](#)).

The Turnbull Ridge unit. Considering its morphostratigraphic position, moderate degree of alteration, and the fairly low A/I values, the Turnbull Ridge unit probably corresponds to the upper part of the OHF, more specifically to the Couplet III of [Hearty and Kaufman \(2000\)](#).

Middle Pleistocene units are not extensively represented on Long Island compared to Eleuthera ([Kindler and Hearty, 1995, 1997; Hearty, 1998](#)) where rock bodies of that age are vertically stacked in 20 m-high

sea cliffs. However, these units form the spine of the south-central part of Long Island, and if the platform margin happened to collapse in this area, as it apparently did in North Eleuthera ([Mullins and Hine, 1989; Kindler and Hine, 2009](#)), similar exposures of middle Pleistocene rocks might be created there.

5.1.2. Late Pleistocene units

The Little Harbour unit. Other outcrops of fossil reefs have been reported from the Stella Maris area ([Curran et al., 2004](#)) and, more recently, from Old Gray, South Point, the embayment to the south of Little Harbour, and Steven's Bluff on the lagoon side of the island ([Dumitru et al., 2023](#)). The latter authors present twelve high-precision U-Th ages that average at *ca.* 122 ka BP, which corresponds with our own data. The Little Harbour unit can confidently be correlated with the CTM reefs. Nevertheless, the presence of a bindstone cap over the coral framestone/rudstone appears to be a specificity of this unit, as such caps do not occur at the most studied exposures of the CTM on San Salvador and Great Inagua ([Chen et al., 1991; Skrivanek et al., 2018](#)). As mentioned in Section 4.4., and like the CTM, the Little Harbour unit locally comprises two phases of coral growth that will be discussed in Section 5.3.

The Deadman's Cay unit. [Hearty \(2010\)](#) also examined exposures of this unit at several localities on Long Island, and measured A/I ratios that average at 0.420 ± 0.024 (*n* = 7). This value is 0.070 higher than ours, possibly because our A/I ratios were not directly measured, but calculated from D/L Val ([Whitacre et al., 2017](#)). He assigned also these

oolites to MIS 5e. Considering its overall lithological and sedimentological characteristics and apparent age, the Deadman's Cay unit can thus be safely correlated with the GBF or with the Couplet IV of [Hearty and Kaufman \(2000\)](#). Furthermore, its position above a reef facies ([Fig. 8A](#) and [9A](#)) indicates it was likely deposited in the late part of MIS 5e as the Fernandez Bay member on San Salvador or the Big Cove member on Mayaguana ([Table 5](#)). The lack of lower MIS 5e sediments (*i.e.*, the FBM) is addressed in [Section 5.2](#).

The Dean's Bay unit. [Hearty \(2010\)](#) identified similar outcrops of skeletal eolianites at Mangrove Bush and in the Clarence Town area, and also examined the exposures at Dean's Blue Hole and Bonne Cord. His measured A/I ratios average at 0.306 ± 0.026 ($n = 5$), which agrees with our data. [Hearty \(2010\)](#) also correlated these skeletal eolianites with MIS 5a. Based on its sedimentological and geochemical characteristics, and its position relative to MSL, the Dean's Bay unit can thus be correlated with the WPF.

The MIS 5a eolianites are extensively exposed on Long Island compared to other islands. In addition, both the lower and upper boundaries of this formation are visible at several outcrops, and clearly identify it as an upper Pleistocene unit distinct and younger than the GBF. The long-lasting controversy regarding the presence of MIS 5a deposits in the Bahamas ([Carew and Mylroie, 1994](#); [Hearty and Kindler, 1994](#)) is thus conclusively resolved.

5.1.3. Holocene units

The Buckley Settlement unit. [Hearty \(2010\)](#) identified comparable exposures of oolitic eolianites at Newton Cay, Salt Pond, and Mangrove Bush on the eastern shoreline of Long Island, and also visited the Buckley outcrop. He obtained two ^{14}C ages and eight A/I ratios from these rock bodies that average, respectively, at $6'205 \pm 351$ yBP and 0.098 ± 0.005 . These values are similar to both our ^{14}C and AAR-dating results. The Buckley Settlement unit can be correlated with mid-Holocene NPM defined on San Salvador ([Carew and Mylroie, 1985](#)). Both units are coeval, and bear identical petrographic and sedimentological characteristics. Mid-Holocene eolianites are particularly widespread on Long Island compared to neighboring islands such as Eleuthera (one exposure) and Crooked (nonexistent), which is possibly due to a difference in the width of the windward platforms.

The Stevens Salina unit. Upper Holocene skeletal sediments forming beach to dune successions congruent with MSL have been identified at several locations along the Ocean coast of the island (*e.g.*, at Salt Pond, Dean's Blue Hole, Dunmore Pit), and ^{14}C -dated at $3'762 \pm 64$ yBP by [Hearty \(2010\)](#). [Curran et al. \(2004\)](#) also observed comparable deposits to the east of the Stella Maris airport and at Cape Santa Maria, and correlated them with the HBM. Despite its petrographic difference (oolitic *vs.* skeletal) and a slightly younger age (*ca.* 2'000 yBP), we think that the Stevens Salina unit can also be correlated with the HBM due to the common sedimentological features it shares with the latter.

5.2. The French Bay Member: myth or reality?

As mentioned above, we have correlated the oolitic-peloidal carbonates of LIG age exposed on Long Island (*i.e.*, the Deadman's Cay unit) with (*e.g.*) the Fernandez Bay Member ([Table 5](#)) because these grainstones locally overlie well-dated LIG reefs ([Fig. 8A](#) and [9A](#)). By contrast, we did not recognize, on this island, a rock body comparable to the transgressive-phase FBM, which leads to review the definition of this unit.

The original application of the FBM is from the SW coast of San Salvador Island where the dune cliffs that face onto French Bay were interpreted "to have been deposited during the initial transgressive phase of Grotto Beach sediment deposition" ([Carew and Mylroie, 1985](#), p.16). However, this assertion was subsequently challenged by [Titus \(1987\)](#) who did not recognize any transgressive member in the GBF, and considered that the deposits placed in the FBM actually overlie the CTM reefs. Later on, [Carew and Mylroie \(1995a\)](#) argued that the FBM displays

all the erosional and depositional characters of the transgressive-phase eolianites depicted in their model of island development, and that it is also analogous to the mid-Holocene NPM on which corals presently grow. The value of this analogy is debatable. Firstly, the NPM is volumetrically insignificant compared to the rock bodies assigned to the FBM that allegedly form "prominent interior dune ridges" on San Salvador ([Carew and Mylroie, 1985](#)). Secondly, the *ca.* 5 ka-old NPM dunes are being actively eroded by marine processes today ([Fig. 9C](#)), and will likely be reduced to a mere lag deposit by the end of the present interglacial highstand. Furthermore, if appropriate, this comparison implies that the substrate of LIG reefs should mainly correspond to an oolitic eolianite of early MIS 5e age. However, at the few localities where it has been observed, and contrary to [Carew and Mylroie's \(1997\)](#) assertion, the unit underlying the CTM can definitely be related to the middle Pleistocene OHF. Such is the case in Abaco ([Hearty and Kindler, 1993b](#); [Hearty et al., 2007](#)), at Grotto Beach and at Crab Cay in San Salvador ([Titus, 1980](#); [Hattin and Warren, 1989](#)), in Great Inagua ([Kindler et al., 2007](#)), Crooked ([Godefroid and Kindler, 2016](#)), West Caicos ([Kerans et al., 2019](#)), and in the Exumas ([Hearty and Backstrom, 2021](#)). In Mayaguana, the CTM reefs are even anchored on marine deposits of early Pleistocene age ([Godefroid, 2011](#)). Moreover, drilling at the type section of the CTM on San Salvador revealed the presence of a paleosol-capped and diagenetically altered reef below the LIG corals at a depth of 9.4 m ([Gose et al., 1999](#)). No trace of a transgressive eolianite was found between the two reefs in these cores. Effectively, [Carew and Mylroie \(1989, 1995a\)](#) observed an oolitic eolianite below the CTM on High Cay (South Andros), and assigned it to the FBM because of the lack of an intervening paleosol. However, this eolianite has never been dated, and this observation was made before the discovery of oolitic grainstones of middle Pleistocene age in the Bahamas. Furthermore, the absence of a paleosol can easily be explained by marine erosion, as is the case at the Boiling Hole (Eleuthera) where the boundary between the OHF and the overlying GBF is razor sharp, and devoid of pedogenic microstructures ([Kindler and Hearty, 1995](#), *their Fig. 4B*). In Bermuda, an island group often compared to the Bahamas, the stratigraphic record includes shallowing-upward carbonate units separated by *terra-rossa* paleosols ([Vacher and Rowe, 1997](#); [Hearty, 2002](#)). Transgressive-phase sediments are represented by "erosional-coastline marine deposits" ([Vacher and Rowe, 1997](#), *their Figs. 2–9*), not by eolianites. Additionally, in the neighboring and geologically similar Yucatan Peninsula, the LIG stratigraphic record comprises from base to top (1) reefal deposits and (2) a regressive succession of predominantly oolitic-peloidal grainstones ([Ward and Brady, 1979](#); [Blanchon, 2010](#); [Shaw, 2016](#)) bounded by paleosols. Transgressive eolianites are likewise missing or poorly exposed. A similar and coeval succession of facies was recently identified by detailed surface and subsurface investigations in the SW part of San Salvador ([Nolting et al., 2023](#)).

To conclude, there is a lack of data available on the FBM in formally published literature that demonstrates any clear relationship to a sea-level transgression. Furthermore, the stratigraphic record of areas geologically comparable to the Bahamas obviously lack transgressive eolianites. Consequently, the hypothesis formulated by [Titus \(1980\)](#) stating that "cyclical sea-level changes produce asymmetrical sedimentary cycles", and that "soft transgressive sequences become reworked and cemented into a permanent regressive facies pattern" should be reevaluated as it seems to better portray the stratigraphic scheme of the Bahamas than the model proposed by [Carew and Mylroie \(1995a, 1997\)](#).

5.3. RSL on long island during the LIG

The paucity markers and the small number of our U-Th ages, both preclude detailed interpretations of the RSL history on Long Island during the LIG. We will thus limit ourselves to provide some constraints on the maximum RSL elevation and possible fluctuations during MIS 5e ([Table 6](#)).

As detailed in sections [4.4.](#) and [4.5.](#), the type section of the Little

Table 6

Determination of LIG RSL on long island during the LIG.

Unit	Sample #	RSL marker	D.P.	Age (ka)	UL (m)	LL (m)	IR (m)	RWL (m)	Elev. (m)	δ Elev. (m)	RSL (m)	δ RSL (m)
DCU	LV 165	b/d Deadman's		<115	2	0	2	1	2.5	0.25	1.5	1
DCU	LV 9	b/d Clarence		<115	2	0	2	1	1	0.1	0	1
DCU	LI 42	beach Little Harbour		114.8 ± 2.2	0.4	-0.4	0.8	0	1	0.1	1	0.4
LHU	LI 39	Ps. aff. clivosa	2	119.7 ± 3.9	-1	-9.1	8.1	-5.05	1.5	0.15	6.55	4.05
LHU	LI 43	Pseudodiploria sp.	2	121.9 ± 2.5	-1.5	-13.4	11.9	-7.45	1	0.1	8.45	5.95
LHU	LI 62	Ps. strigosa	2	117.2 ± 2.2	-1.5	-13.4	11.9	-7.45	0	0.1	7.45	5.95
LHU	LI 104	Ps. strigosa	2	119.0 ± 2.0	-1.5	-13.4	11.9	-7.45	0	0.1	7.45	5.95
LHU	LV 31	patch reef DB	1	122.0 ± 1.5	0	-6	6	-3	1.5	0.15	4.5	3
LHU	LI 103	patch reef DB	1	122.3 ± 3.2	0	-6	6	-3	1.5	0.15	4.5	3
LHU	LI 37	bindstone	1	ca. 122.0	-0.2	-0.6	0.4	-0.4	2.5	0.25	2.9	0.2
LHU	LI 77	P. asteroides	1	124.6 ± 1.6	0	-6	6	-3	0	0.5	3	3
LHU	LI 130	A. cervicornis	1	121.5 ± 2.5	0	-6	6	-3	0	0.5	3	3

DCU = Deadman's Cay unit; LHU = Little Harbour Unit; D.P. = depositional phase; UL = upper limit of indicator; LL = lower limit of indicator.

IR = indicative range; RWL = reference water level; Elev. = elevation; δ Elev. = elevation error; RSL = relative sea level; δ RSL = error on RSL.

b/d = beach - dune contact.

Harbour unit displays two phases of reef growth overlain by beach sediments assigned to the Deadman's Cay unit. The first growth phase comprises the coral core of the bioherms and the capping algal bindstone, the second one is represented by the *Pseudodiploria* sp. colonies that overlie the bindstone. The age of the first phase can be estimated between 126.2 and 123.0 ka BP, that of the second phase between 122.0 and 117.2 ka BP, and that of the capping beach facies between 117.0 and 112.6 ka BP (Tables 3 and 6). The most precise RSL stand during the first growth phase is derived from the elevation of the algal bindstone at $+2.90 \pm 0.2$ m (Table 6). For the second phase, the best estimate is evaluated at $+6.55 \pm 4.05$ m from the position of the *P. clivosa* colony (Table 6). Finally, the beach sediments indicate a paleo RSL datum at $+1.0 \pm 0.4$ m. Possibly coeval with the algal cap exposed at Little Harbour, the patch reef at Dean's Bay points towards a paleo RSL at $+4.5 \pm 3.0$ m, whereas an elevation between 0 and $+1.5$ m can be calculated from the beach/dune contacts at the Deadman's Cay and Clarence Town exposures that have not been precisely dated.

Relying on our geochronological and sedimentological data, we can thus hypothesize that RSL hovered around $+3$ m in the first part of the LIG, rose by 2–3 m in the middle of this time period, and began its descent to subglacial levels about 115 kyrs ago. Our conservative estimate of this mid-LIG rise is based on the overall encrusting morphology of the *Pseudodiploria* sp. colonies capping the algal bindstone (Fig. 7C) which argues for limited accommodation space. Furthermore, the lack of pedogenic features at the top of the bindstone (Fig. 7D) suggests that this deepening was not preceded by an exposure event.

Our tentative reconstruction of the RSL on Long Island during the LIG generally agrees with that of Dumitru et al. (2023; their Fig. 5) despite the fact that the paleo-water depths assigned to the corals are different. Likewise, these authors did not observe "stratigraphic indications of exposure or significant non-deposition/erosion indicative of a local sea-level oscillation" between the two phases of reef growth. The ages we obtained on these phases agree also with the data of Skrivanek et al. (2018) who recalculated the ages of the two vertically stacked reefs previously identified on Great Inagua and San Salvador islands (Chen et al., 1991; Hearty and Kindler, 1993a; Thompson et al., 2011). The youngest age recorded in their Reef I is 124.5 ± 1.0 ka BP and the ages measured on Reef II range from ca. 123.6 to 119.4 ka BP. These authors derived RSL elevations between $+2.14$ and $+5.02$ m for Reef I and between $+2.14$ and $+6.64$ m for Reef II which do not significantly differ from the values obtained from the reefs at Little Harbour despite the fact that these reefs thrived on distinct islands. Relying on a previous study (Wilson et al., 1998), Skrivanek et al. (2018) argue that the two generations of reef growth are separated by an ephemeral sea-level fall which does not agree with our reconstitution. A scenario similar to ours has also been presented by Blanchon et al. (2009) who deduced a sea-level "jump" from ca. $+3$ to $+6$ m about 121 kyr ago from the architecture of fossil reefs in Yucatan.

To sum up, our geochronological and sedimentological data seem to indicate that, on Long Island, the elevation of RSL was around $+3$ m above MSL during the early part of the LIG, and around $+5$ to $+6$ m near the end of this time interval. About 1.6 m should be added to these values if the subsidence rate estimated by Pierson (1982) for this area happened to be correct. These data further show that the mid-LIG sea-level rise was not preceded by an emergence, and support existing models of glacial isostatic adjustment in the region (Dumitru et al., 2023).

6. Conclusions

We have identified, described, and mapped eight allostratigraphic units on Long Island that range in age from the middle Pleistocene to the late Holocene, and are separated by *terra-rossa* paleosols. These units mostly comprise eolianites, and can generally be correlated with the members and formations previously defined on other Bahamian islands. However, the Buckley Settlement and the Dean's Bay units, respectively equivalents of the NPM and of the WPF, are more widespread on Long Island than on other islands, possibly due to differences in the width of the windward shelves. Furthermore, we could not identify on Long Island an equivalent of the FBM, an extensive rock body supposedly accumulated during the LIG transgression. The lack of such deposits raises questions about the volume and the nature of transgressive sediments that can possibly be preserved during a sea-level cycle in the Bahamas, and leads to reconsider previously proposed models of Bahamian islands development. Finally, the examination and, in some cases, the dating of paleo sea-level markers suggest that, without taking account of the potential subsidence, RSL on Long Island was about $+3$ m above modern datum in the first half of the LIG, and rose to about $+5$ m in the middle of this period. This rise was likely not preceded by an exposure event.

Credit authorship contribution statement

Lucas Vimpere: Conceptualization, Methodology, Formal analysis, Investigation, Resources, Writing - Original Draft, Writing - Review & Editing, Visualization, Supervision, Project administration.

Pascal Kindler: Conceptualization, Methodology, Investigation, Writing - Original Draft, Writing - Review & Editing, Supervision, Project administration, Funding acquisition.

Nabil Shawwa: Investigation, Resources, Writing - Review & Editing.

Giovan Peyrotty: Writing - Original Draft, Writing - Review & Editing.

Sébastien Castelltort: Supervision, Project administration, Funding acquisition.

Data availability statement

The data that support the findings of this study are available from the corresponding author upon reasonable request.

Declaration of competing interest

The authors declare that they have no known competing financial interests or personal relationships that could have appeared to influence the work reported in this paper.

Acknowledgements

We thank F. Gischig (University of Geneva) for thin-section manufacturing, Prof. D.S. Kaufman (Northern Arizona University) for amino-acid racemization data, PhD G. Bassam and Prof. S. Sanderson (GEOTOP-UQAM) for U-Th data. Our expenses were supported by the Swiss National Science Foundation (grants n° 200020-124608/1 and 200020-140420/1) and by the Department of Earth Sciences of the University of Geneva. Fieldwork pertaining to this study was carried out in 2014, 2015, and 2018, that is before the Bahamian Government completely re-wrote their research permit system to a much more stringent and rigorous standard. At the time, a permit was only required if research was performed in National Parks, which was not our case. TanDEM-X DEM is under copyright by the German Aerospace Centre (DLR) and was used with permission. We acknowledge the IGGT research group of the University of Geneva for their efficiency and for their helpful discussions of the results, and we are grateful to the editor and an unknown reviewer for constructive comments on earlier manuscript.

Appendix A. Supplementary data

Supplementary data to this article can be found online at <https://doi.org/10.1016/j.quascirev.2025.109640>.

Data availability

All data and/or code is contained within the submission.

References

- Barlow, N.L.M., McClymont, E.L., Whitehouse, P.L., Stokes, C.R., Jamieson, S.S.R., Woodroffe, S.A., Bentley, M.J., Louise Callard, S.L., Cofaigh, C.Ó., Evans, D.J.A., Horrocks, J.R., Lloyd, J.M., Long, A.J., Margold, M., Roberts, D.H., Sanchez-Montes, M.L., 2018. Lack of evidence for a substantial sea-level fluctuation within the Last Interglacial. *Nat. Geosci.* 11, 627–634. <https://doi.org/10.1038/s41561-018-0195-4>.
- Blanchon, P., 2010. Reef demise and back-stepping during the last interglacial, northeast Yucatan. *Coral Reefs* 29, 481–498. <https://doi.org/10.1007/s00338-010-0599-0>.
- Blanchon, P., Eisenhauer, A., Fietzke, J., Liebetrau, V., 2009. Rapid sea-level rise and reef back-stepping at the close of the last interglacial highstand. *Nature* 458, 881–885. <https://doi.org/10.1038/nature07933>.
- Bretz, J.H., 1960. Bermuda: a partially drowned, late mature, Pleistocene karst. *Geol. Soc. Am. Bull.* 71, 1729–1754. [https://doi.org/10.1130/0016-7606\(1960\)71\[1729:BADPLM\]2.0.CO;2](https://doi.org/10.1130/0016-7606(1960)71[1729:BADPLM]2.0.CO;2).
- Bush, S.L., Santos, G.M., Xu, X., Southon, J.R., Thiagarajan, N., Hines, S.K., Adkins, J.F., 2013. Simple, rapid, and cost effective: a screening method for ^{14}C analysis of small carbonate samples. *Radiocarbon* 55, 631–640. <https://doi.org/10.1017/S003822200057787>.
- Carew, J.L., Mylroie, J.E., 1985. The Pleistocene and Holocene stratigraphy of San Salvador Island, Bahamas, with reference to marine and terrestrial lithofacies at French Bay. In: Curran, H.A. (Ed.), *Pleistocene and Holocene Carbonate Environments on San Salvador Island, Bahamas: Geological Society of America, Annual Meeting Guidebook, Ft. Lauderdale, FL: CCFL Bahamian Field Station*, pp. 11–61.
- Carew, J.L., Mylroie, J.E., 1989. The geology of eastern South Andros Island, Bahamas: a preliminary report. In: Mylroie, J.E. (Ed.), *Proceedings of the Fourth Symposium on the Geology of the Bahamas, Bahamian Field Station, San Salvador*, pp. 73–81.
- Carew, J.L., Mylroie, J.E., 1994. New perspectives on Bahamian geology: San Salvador, Bahamas. *Discussion of Hearty, P.J., and Kindler, P.*, 1993. *J. Coast Res.* 9, 577–594.
- Carew, J.L., Mylroie, J.E., 1995a. Depositional model and stratigraphy for the Quaternary geology of the Bahama Islands. In: Curran, H.A., White, B. (Eds.), *Terrestrial and Shallow Marine Geology of the Bahamas and Bermuda*, vol. 300. Geological Society of America Special Paper, pp. 5–32. <https://doi.org/10.1130/0-8137-2300-0.5>.
- Carew, J.L., Mylroie, J.E., 1995b. Quaternary tectonic stability of the Bahamian Archipelago: evidence from fossil coral reefs and flank margin caves. *Quat. Sci. Rev.* 14, 145–153. [https://doi.org/10.1016/0277-3791\(94\)00108-N](https://doi.org/10.1016/0277-3791(94)00108-N).
- Carew, J.L., Mylroie, J.E., 1997. Geology of The Bahamas. In: Vacher, H.L., Quinn, T.M. (Eds.), *Geology and Hydrogeology of Carbonate Islands, Developments in Sedimentology*, vol. 54. Elsevier, Amsterdam, pp. 91–139. [https://doi.org/10.1016/S0070-4571\(04\)80023-2](https://doi.org/10.1016/S0070-4571(04)80023-2).
- Carter, H.E., Warwick, P., Cobb, J., Longworth, G., 1999. Determination of uranium and thorium in geological materials using extraction chromatography. *Analyst* 124, 271–274. <https://doi.org/10.1039/a809781j>.
- Chen, J.H., Curran, H.A., White, B., Wasserburg, G.J., 1991. Precise chronology of the last interglacial period: ^{234}U - ^{230}Th data from fossil coral reefs in the Bahamas. *Geol. Soc. Am. Bull.* 103, 82–97. [https://doi.org/10.1130/0016-7606\(1991\)103<0082:PCOTLI>2.3.CO;2](https://doi.org/10.1130/0016-7606(1991)103<0082:PCOTLI>2.3.CO;2).
- Chutcharavan, P.M., Dutton, A., 2021. A global compilation of U-series-dated fossil coral sea-level indicators for the Last Interglacial period (Marine Isotope Stage 5e). *Earth Syst. Sci. Data* 13, 3155–3178. <https://doi.org/10.5194/esd-13-3155-2021>.
- Clark, P.U., Huybers, P., 2009. Interglacial and future sea level. *Nature* 462, 856–857. <https://doi.org/10.1038/462856a>.
- Curran, H.A., Mylroie, J.E., Gamble, D.W., Wilson, M.A., Davis, R.L., Sealey, N.E., Voegeli, V.J., 2004. *Geology of Long Island, Bahamas: a field trip guide. Fieldtrip Guidebook, 12th Symposium on the Geology of the Bahamas and Other Carbonate Regions*. Gerace Research Centre, San Salvador, Bahamas, p. 24.
- Davaud, E., Strasser, A., 1984. Progradations, cimentations, érosion: évolution sédimentaire et diégénétique récente d'un littoral carbonaté (Bimini, Bahamas). *Eclogae Geol. Helv.* 77, 449–468. <https://doi.org/10.5169/seals-165517>.
- Dolan, J.F., Mullins, H.T., Wald, D.J., 1998. Active tectonics of the north-central Caribbean: oblique collision, strain partitioning and opposing subducted slabs. In: Dolan, J.F., Mann, P. (Eds.), *Active Strike-Slip and Collisional Tectonics of the Northern Caribbean Plate Boundary Zone*, vol. 326. Geological Society of America Special Paper, pp. 1–61.
- Dumitru, O.A., Dyer, B., Austermann, J., Sandstrom, M.R., Goldstein, S.L., D'Andrea, W.J., Cashman, M., Creel, R., Bolge, L., Raymo, M.E., 2023. Last interglacial global mean sea level from high-precision U-series ages of Bahamian fossil coral reefs. *Quat. Sci. Rev.* 318. <https://doi.org/10.1016/j.quascirev.2023.108287>.
- Dutton, A., Villa, A., Chutcharavan, P.M., 2022. Compilation of last Interglacial (Marine Isotope Stage 5e) sea-level indicators in The Bahamas, Turks and Caicos, and the east coast of Florida, USA. *Earth Syst. Sci. Data* 14 (5), 2385–2399. <https://doi.org/10.5194/esd-14-2385-2022>.
- Dyer, B., Austermann, J., D'Andrea, W.J., Creel, R.C., Sandstrom, M.R., Cashman, M., Rovere, A., Raymo, M.E., 2021. Sea-Level Trends Across the Bahamas Constrain Peak Last Interglacial Ice Melt, vol. 118. *Proceedings of the National Academy of Sciences*. <https://doi.org/10.1073/pnas.2026839118>.
- Fouke, K.W., Kerans, C., 2024. Evidence for a sea level fall during the Last Interglacial highstand on West Caicos, Turks and Caicos Islands. *Paleoceanogr. Paleoclimatol.* 39, e2024PA004879. <https://doi.org/10.1029/2024PA004879>.
- Garrett, P., Gould, S.J., 1984. Geology of New Providence Island, Bahamas. *Geol. Soc. Am. Bull.* 95, 209–220. [https://doi.org/10.1130/0016-7606\(1984\)95<209:GONPIB>2.0.CO;2](https://doi.org/10.1130/0016-7606(1984)95<209:GONPIB>2.0.CO;2).
- Godefroid, F., 2011. *Géologie De Mayaguana, SE De L'Archipel Des Bahamas* (Ph.D. Thesis). University of Geneva, Switzerland. <https://doi.org/10.13097/archiveouverte/unige:20295>.
- Godefroid, F., Kindler, P., 2016. Prominent geological features of Crooked Island, SE Bahamas. In: Glumac, B., Savarese, M. (Eds.), *Proceedings of the 16th Symposium on the Geology of the Bahamas and Other Carbonate Regions*. Gerace Research Center, San Salvador, Bahamas, pp. 26–38.
- Godefroid, F., Kindler, P., Chiaradia, M., Fischer, J., 2019. The Misery Point cliff, Mayaguana Island, SE Bahamas: a unique record of sea-level highstands since the early Pleistocene. *Swiss J. Geosci.* 112, 287–305. <https://doi.org/10.1007/s00015-018-0323-6>.
- Gose, L.R., Carney, C.R., Boardman, M.R., 1999. A core-based depositional interpretation of Cockburn Town, San Salvador Island, Bahamas. In: Curran, H.A., Mylroie, J.E. (Eds.), *Proceedings of the Ninth Symposium on the Geology of the Bahamas and Other Carbonate Regions*. Bahamas Field Station, San Salvador, Bahamas, pp. 69–80.
- Halley, R.B., Harris, P.M., 1979. Fresh-water cementation of a 1'000-year-old oolite. *J. Sediment. Petrol.* 49, 969–988. <https://doi.org/10.1306/212F7892-2B24-11D7-8648000102C1865D>.
- Hattin, D.E., Warren, V.L., 1989. Stratigraphic analysis of a fossil *Neogoniolithon*-capped patch reef and associated facies, San Salvador, Bahamas. *Coral Reefs* 8, 19–30. <https://doi.org/10.1007/BF00304688>.
- Hearty, P.J., 1998. The geology of Eleuthera Island, Bahamas: a Rosetta stone of Quaternary stratigraphy and sea-level history. *Quat. Sci. Rev.* 17, 333–355. [https://doi.org/10.1016/S0277-3791\(98\)00046-8](https://doi.org/10.1016/S0277-3791(98)00046-8).
- Hearty, P.J., 2002. Revision of the late Pleistocene stratigraphy of Bermuda. *Sediment. Geol.* 153, 1–21. [https://doi.org/10.1016/S0037-0738\(02\)00261-0](https://doi.org/10.1016/S0037-0738(02)00261-0).
- Hearty, P.J., 2010. Chronostratigraphy and morphological changes in *cerion* land snail shells over the past 130 ka on Long Island, Bahamas. *Quat. Geochronol.* 5, 50–64. <https://doi.org/10.1016/j.quageo.2009.09.005>.
- Hearty, P.J., Backstrom, J.T., 2021. Surficial and shallow subsurface geology of the Northern and Central Exuma Cays, The Bahamas. *Caribb. J. Sci.* 51, 264–286. <https://doi.org/10.18475/cjs.v51i2.a12>.

- Hearty, P.J., Hollin, J.T., Neumann, A.C., O'Leary, M.J., McCulloch, M., 2007. Global sea-level fluctuations during the last Interglaciation (MIS 5e). *Quat. Sci. Rev.* 26, 2090–2112. <https://doi.org/10.1016/j.quascirev.2007.06.019>.
- Hearty, P.J., Kaufman, D.S., 2000. Whole-rock aminostratigraphy and Quaternary sea-level history of The Bahamas. *Quat. Res.* 54, 163–173. <https://doi.org/10.1006/qres.2000.2164>.
- Hearty, P.J., Kaufman, D.S., 2009. A *Cerion*-based chronostratigraphy and age model from the central Bahama Islands: amino acid racemization and ^{14}C in land snails and sediments. *Quat. Geochronol.* 4, 148–159. <https://doi.org/10.1016/j.quageo.2008.08.002>.
- Hearty, P.J., Kindler, P., 1993a. New perspectives on Bahamian geology: San Salvador Island, Bahamas. *J. Coast. Res.* 9, 577–594.
- Hearty, P.J., Kindler, P., 1993b. An illustrated stratigraphy of the Bahama Islands: in search of a common origin. *Bahamas J. Sci.* 1, 28–45.
- Hearty, P.J., Kindler, P., 1994. Straw men, glass houses, apples and oranges: a response to Carew and Mylroie's comment on Hearty and Kindler (1993). *J. Coast. Res.* 10, 1095–1104.
- Hearty, P.J., Kindler, P., 1997. The stratigraphy and surficial geology of New Providence and surrounding Islands, Bahamas. *J. Coast. Res.* 13, 798–812.
- Hearty, P.J., Kindler, P., Cheng, H., Edwards, R.L., 1999. A +20 m middle Pleistocene sea-level highstand (Bermuda and The Bahamas) due to partial collapse of Antarctic ice. *Geology* 27, 375–378. [https://doi.org/10.1130/0091-7613\(1999\)027<0375:AMMPSL>2.3.CO;2](https://doi.org/10.1130/0091-7613(1999)027<0375:AMMPSL>2.3.CO;2).
- Hearty, P.J., Neumann, A.C., 2001. Rapid sea level and climate change at the close of the last Interglaciation (MIS 5e): evidence from the Bahama Islands. *Quat. Sci. Rev.* 20, 1881–1895. [https://doi.org/10.1016/S0277-3791\(01\)00021-X](https://doi.org/10.1016/S0277-3791(01)00021-X).
- Hibbert, F.D., Rohling, E.J., Dutton, A., Williams, F.H., Chutcharavan, P.M., Zhao, C., Tamisiea, M.E., 2016. Coral indicators of past sea-level change: a global repository of U-series dated benchmarks. *Quat. Sci. Rev.* 145, 1–56. <https://doi.org/10.1016/j.quascirev.2016.04.019>.
- Horwitz, E.Ph., Dietz, M.L., Chiarizia, R., 1992. The application of novel extraction chromatographic materials to the characterization of radioactive waste solutions. *J. Radioanal. Nucl. Chem. Article.* 161, 575–583. <https://doi.org/10.1007/BF02040504>.
- Howarth, R.J., McArthur, J.M., 1997. Statistics for strontium isotope stratigraphy: a robust lowess fit to the marine Sr-isotope curve for 0 to 206 Ma, with look-up table for derivation of numeric age. *J. Geol.* 105, 441–456. <https://doi.org/10.1086/515938>.
- Itzhaki, Y., 1961. Pleistocene Shorelines in the Coastal Plains of Israel, vol. 32. Geological Survey of Israel Bulletin, pp. 1–9.
- Jackson, K.L., 2017. Sedimentary record of Holocene and Pleistocene sea-level oscillations in the Exuma Cays and New Providence, Bahamas (Ph.D. Thesis). University of Miami, p. 506. <https://scholarship.miami.edu/esploro/outputs/doctr/Sedimentary-Record-of-Holocene-and-Pleistocene/991031447839702976>.
- Kaufman, D.S., Manley, W.F., 1998. A new procedure for determining DL amino acid ratios in fossils using reverse phase liquid chromatography. *Quat. Sci. Rev.* 17, 987–1000. [https://doi.org/10.1016/S0277-3791\(97\)00086-3](https://doi.org/10.1016/S0277-3791(97)00086-3).
- Kerans, C., Zahm, C., Bachtel, S.L., Hearty, P., Cheng, H., 2019. Anatomy of a late Quaternary carbonate island: constraints on timing and magnitude of sea-level fluctuations, West Caicos, Turks and Caicos Islands, BWI. *Quat. Sci. Rev.* 205, 193–223. <https://doi.org/10.1016/j.quascirev.2018.12.010>.
- Kindler, P., 1992. Coastal response to the Holocene transgression in The Bahamas: episodic sedimentation versus continuous sea-level rise. *Sediment. Geol.* 80, 319–329. [https://doi.org/10.1016/0037-0738\(92\)90049-W](https://doi.org/10.1016/0037-0738(92)90049-W).
- Kindler, P., Godefroid, F., Chiaradia, M., Ehler, C., Eisenhauer, A., Frank, M., Hasler, C.-A., Samankassou, E., 2011. Discovery of Miocene to early Pleistocene deposits on Mayaguana, Bahamas: evidence for recent active tectonism on the North American margin. *Geology* 39, 523–526. <https://doi.org/10.1130/G32011.1>.
- Kindler, P., Hearty, P.J., 1995. Pre-Sangamonian eolianites in The Bahamas? New evidence from Eleuthera Island. *Mar. Geol.* 127, 73–86. [https://doi.org/10.1016/0025-3227\(95\)00052-Z](https://doi.org/10.1016/0025-3227(95)00052-Z).
- Kindler, P., Hearty, P.J., 1996. Carbonate petrography as an indicator of climate and sea-level changes: new data from Bahamian Quaternary units. *Sedimentology* 43, 381–399. <https://doi.org/10.1046/j.1365-3091.1996.d01-11.x>.
- Kindler, P., Hearty, P.J., 1997. Geology of The Bahamas: architecture of Bahamian Islands. In: Vacher, H.L., Quinn, T.M. (Eds.), *Geology and Hydrogeology of Carbonate Islands, Developments in Sedimentology*, vol. 54, pp. 141–160. [https://doi.org/10.1016/S0070-4571\(04\)80024-4](https://doi.org/10.1016/S0070-4571(04)80024-4).
- Kindler, P., Hearty, P.J., 2022. The Whale Point Formation: a stratigraphic record of high-frequency climate and sea-level fluctuations in The Bahamas during Marine Isotope Stage 5a (ca. 80 ka BP). *Sediment. Geol.* 432. <https://doi.org/10.1016/j.sedgeo.2022.106107>.
- Kindler, P., Hine, A.C., 2009. The paradoxical occurrence of oolitic limestone on the eastern islands of Great Bahama Bank: where do the ooids come from?. In: Swart, P. K., Eberli, G.P., McKenzie, J.A. (Eds.), *Perspectives in Carbonate Geology: A Tribute to the Career of Robert Nathan Ginsburg*, vol. 41. IAS Special Publication, pp. 113–122. <https://doi.org/10.1002/9781444312065.ch8>.
- Kindler, P., Reiss, J.-L., Cazala, C., Plagnes, V., 2007. Discovery of a composite reefal terrace of middle and late Pleistocene age in Great Inagua Island, Bahamas. Implications for regional tectonics and sea-level history. *Sediment. Geol.* 194, 141–147. <https://doi.org/10.1016/j.sedgeo.2006.05.027>.
- Kopp, R.E., Simons, F.J., Mitrovica, J.X., Maloof, A.C., Oppenheimer, M., 2013. A probabilistic assessment of sea level variations within the last interglacial stage. *Geophys. J. Int.* 193, 711–716. <https://doi.org/10.1093/gji/ggt029>.
- Land, L.S., MacKenzie, F.T., Gould, S.J., 1967. Pleistocene history of Bermuda. *Geol. Soc. Am. Bull.* 78, 993–1006. [https://doi.org/10.1130/0016-7606\(1967\)78\[993:PHOB\]2.0.CO;2](https://doi.org/10.1130/0016-7606(1967)78[993:PHOB]2.0.CO;2).
- Linge, H., Lauritzen, S.-E., Mangerud, J., Kamenos, N.A., Gherardi, J.M., 2008. Assessing the use of U-Th methods to determine the age of cold-water calcareous algae. *Quat. Geochronol.* 3, 76–88. <https://doi.org/10.1016/j.quageo.2007.09.003>.
- Lisiecki, L.E., Raymo, M.E., 2005. A Pliocene-Pleistocene stack of 57 globally distributed benthic $\delta^{18}\text{O}$ records. *Paleoceanography* 20. <https://doi.org/10.1029/2004PA001071>.
- Lynts, G.W., 1970. Conceptual model of the Bahamian platform for the last 135 million years. *Nature* 225, 1226–1228. <https://doi.org/10.1038/2251226a0>.
- Masaferro, J.L., Poblet, J., Bulnes, M., Eberli, G.P., Dixon, T.H., McClay, K., 1999. Palaeogene-Neogene/present day(?) growth folding in the Bahamian foreland of the Cuban fold and thrust belt. *J. Geol. Soc.* 156, 617–631. <https://doi.org/10.1144/gsjgs.156.3.0617>. London.
- McArthur, J.M., Howarth, R.J., Bailey, T.R., 2001. Strontium isotope stratigraphy: LOWESS Version 3: best fit to the marine Sr-isotope curve for 0–509 Ma and accompanying look-up table for deriving numerical age. *J. Geol.* 109, 155–170. <https://doi.org/10.1086/319243>.
- McArthur, J.M., Howarth, R.J., Shields, G.A., Zhou, Y., 2020. Chapter 7 - strontium isotope stratigraphy. In: Gradstein, F.M., Ogg, J.G., Schmitz, M.D., Ogg, G.M. (Eds.), *Geologic Time Scale 2020*, pp. 211–238. <https://doi.org/10.1016/B978-0-12-824360-2.00007-3>.
- Meyerhoff, A.A., Hatten, C.W., 1974. Bahamas salient of North America: tectonic framework, stratigraphy, and petroleum potential. *AAPG (Am. Assoc. Pet. Geol.) Bull.* 58, 1201–1239. <https://doi.org/10.1306/83D9164B-16C7-11D7-8645000102C1865D>.
- Mulder, T., Ducassou, E., Gillet, H., Hanquiez, V., Tournadour, E., Combes, J., Eberli, G. P., Kindler, P., Gonthier, E., Conesa, G., Robin, C., Sianipar, R., Reijmer, J.J.G., François, A., 2012. Canyon morphology on a modern carbonate slope of The Bahamas: evidence of regional tectonic tilting. *Geology* 40, 771–774. <https://doi.org/10.1130/G33327.1>.
- Muhs, D.R., Bush, C.A., 1987. Uranium-series age determinations of Quaternary eolianites and implications for sea-level history. In: *New Providence Islands, Bahamas*. Geological Society of America Abstracts with Programs, 19/7, p. 780.
- Muhs, D.R., Bush, C.A., Stewart, K.C., Rowland, T.R., Crittenden, R.C., 1990. Geochemical evidence of Saharan dust parent material for soils developed on Quaternary limestones of Caribbean and Western Atlantic islands. *Quat. Res.* 33, 157–177. [https://doi.org/10.1016/0033-5894\(90\)90016-E](https://doi.org/10.1016/0033-5894(90)90016-E).
- Muhs, D.R., Simmons, K.R., Schumann, R.R., Schweig, E.S., Rowe, M.P., 2020. Testing glacial isostatic adjustment models of last-interglacial sea level history in The Bahamas and Bermuda. *Quat. Sci. Rev.* 233. <https://doi.org/10.1016/j.quascirev.2020.106212>.
- Mullins, H.T., Hine, A.C., 1989. Scalloped bank margins: beginning of the end for carbonareous platforms? *Geology* 17, 30–33. [https://doi.org/10.1130/0091-7613\(1989\)017<0030:SBMBOT>2.3.CO;2](https://doi.org/10.1130/0091-7613(1989)017<0030:SBMBOT>2.3.CO;2).
- Mullins, H.T., Lynts, G.W., 1977. Origin of the northwestern Bahama Platform: review and reinterpretation. *Geol. Soc. Am. Bull.* 88, 1447–1461. [https://doi.org/10.1130/0016-7606\(1977\)88<1447:OOTNBP>2.0.CO;2](https://doi.org/10.1130/0016-7606(1977)88<1447:OOTNBP>2.0.CO;2).
- Mylroie, J.E., Carew, J.L., Sealey, N.E., Mylroie, J.R., 1991. Cave development on New Providence Island and Long Island, Bahamas. *Cave Sci.* 18, 139–151.
- Mylroie, J.E., 2008. Late Quaternary sea-level position: evidence from Bahamian carbonate deposition and dissolution cycles. *Quat. Int.* 183, 61–75. <https://doi.org/10.1016/j.quaint.2007.06.030>.
- Neumann, A.C., Hearty, P.J., 1996. Rapid sea-level changes at the close of the last interglacial (substage 5e) recorded in Bahamian island geology. *Geology* 24, 775–778. [https://doi.org/10.1130/0091-7613\(1996\)024<0775:RSLCAT>2.3.CO;2](https://doi.org/10.1130/0091-7613(1996)024<0775:RSLCAT>2.3.CO;2).
- Neumann, A.C., Moore, W.S., 1975. Sea level events and Pleistocene coral ages in the Northern Bahamas. *Quat. Res.* 5, 215–224. [https://doi.org/10.1016/0033-5894\(75\)90024-1](https://doi.org/10.1016/0033-5894(75)90024-1).
- Nolting, A., Kerans, C., Fernandez-Ibanez, F., Fullmer, S., Moore, P.J., Breithaupt, C.I., LeBlanc, S., Dafoe, M., Bunge, E., Gulley, J., 2023. Three-dimensional stratigraphic architecture, secondary pore system development and the middle Pleistocene transition, Sandy Point area, San Salvador Island, Bahamas. *Sedimentology* 71, 207–240. <https://doi.org/10.1111/sed.13134>.
- North American Commission on Stratigraphic Nomenclature, 2021. North American stratigraphic code. *Stratigraphy* 18, 153–204. <https://doi.org/10.29041/strat.18.3.01>.
- Pierson, B.J., 1982. *Cyclic Sedimentation, Limestone Diagenesis and Dolomitization in Upper Cenozoic Carbonates of the Southeastern Bahamas* (Ph.D. Thesis). University of Miami, Florida, USA, p. 286.
- Reid, S.B., 2010. The Complex Architecture of New Providence Island (Bahamas) Built by Multiple Pleistocene Sea Level Highstands (M.Sc. Thesis). University of Miami, Florida, p. 199. <http://scholarlyrepository.miami.edu/oa/thesis/77>.
- Rovere, A., Raymo, M.E., Vacchi, M., Lorscheid, T., Stocchi, P., Gómez-Pujol, L., Harris, D.L., Casella, E., O'Leary, M.J., Hearty, P.J., 2016. The analysis of Last Interglacial (MIS 5e) relative sea-level indicators: reconstructing sea-level in a warmer world. *Earth Sci. Rev.* 159, 404–427. <https://doi.org/10.1016/j.earscirev.2016.06.006>.
- Rowe, M.P., Bristow, C.S., 2015. Landward-advancing Quaternary eolianites of Bermuda. *Aeolian Res.* 19, 235–249. <https://doi.org/10.1016/j.aeolia.2015.06.007>.
- Sealey, K.S., Logan, A., 2019. The Commonwealth of The Bahamas. In: *World Seas: an Environmental Evaluation*. Academic Press, pp. 591–615. <https://doi.org/10.1016/B978-0-12-805068-2.00030-9>.

- Shaw, C.E., 2016. Late Pleistocene bays and reefs: ancestors to the modern Caribbean coast, Yucatan Peninsula, Mexico. *J. Coast Res.* 32, 280–285. <https://doi.org/10.2112/JCOASTRES-D-14-00083.1>.
- Shipper, K., Mann, P., 2024. Crustal structure, deformational history, and tectonic origin of The Bahamas carbonate platform. *G-cubed* 25, e2023GC011300. <https://doi.org/10.1029/2023GC011300>.
- Skrivanek, A., Li, J., Dutton, A., 2018. Relative sea-level change during the Last Interglacial as recorded in Bahamian fossil reefs. *Quat. Sci. Rev.* 200, 160–177. <https://doi.org/10.1016/j.quascirev.2018.09.033>.
- Stirling, C.H., Esat, T.M., Lambbeck, K., McCulloch, M.T., 1998. Timing and duration of the last Interglacial: evidence for a restricted interval of widespread coral reef growth. *Earth Planet Sci. Lett.* 160, 745–762. [https://doi.org/10.1016/S0012-821X\(98\)00125-3](https://doi.org/10.1016/S0012-821X(98)00125-3).
- Stuiver, M., Polach, H.A., 1977. Discussion reporting of ^{14}C data. *Radiocarbon* 19 (3), 355–363. <https://doi.org/10.1017/S0033822200003672>.
- Tamura, T., 2012. Beach ridges and prograded beach deposits as palaeoenvironment records. *Earth Sci. Rev.* 114, 279–297. <https://doi.org/10.1016/j.earscirev.2012.06.004>.
- Thompson, W.G., Curran, H.A., Wilson, M.A., White, B., 2011. Sea-level oscillations during the last interglacial highstand recorded by Bahamas corals. *Nat. Geosci.* 4, 684–687. <https://doi.org/10.1038/ngeo1253>.
- Titus, R., 1980. Quaternary emergent facies patterns of San Salvador, Bahamas. In: Gerace, D.T. (Ed.), *Field Guide to the Geology of San Salvador Bahamian Field Station*, pp. 97–116.
- Titus, R., 1983. Quaternary stratigraphy of San Salvador, Bahamas. In: Gerace, D.T. (Ed.), *Proceedings of the First Symposium on the Geology of the Bahamas, CCFL Bahamas Field Station*. San Salvador, pp. 1–5.
- Titus, R., 1987. Geomorphology, stratigraphy, and the Quaternary history of San Salvador. In: Curran, H.A. (Ed.), *Proceedings of the Third Symposium on the Geology of the Bahamas, Bahamian Field Station*. San Salvador, pp. 155–164.
- Uchupi, E., Milliman, J.D., Luyendyk, B.P., Bowin, C.O., Emery, K.O., 1971. Structure and origin of southeastern Bahamas. *AAPG (Am. Assoc. Pet. Geol.) Bull.* 55, 687–704. <https://doi.org/10.1306/819A3C56-16C5-11D7-8645000102C1865D>.
- Vacher, L., 1973. Coastal dunes of younger Bermuda. In: Coates, D.R. (Ed.), *Coastal Geomorphology. Publications in Geomorphology*. State University of New York, pp. 355–391.
- Vacher, H.L., Rowe, M.P., 1997. Geology and hydrogeology of Bermuda. In: Vacher, H.L., Quinn, T.M. (Eds.), *Geology and Hydrogeology of Carbonate Islands, Developments in Sedimentology*, vol. 54. Elsevier, Amsterdam, pp. 35–90. [https://doi.org/10.1016/S0070-4571\(04\)80022-0](https://doi.org/10.1016/S0070-4571(04)80022-0).
- Vimpere, L., 2017. *Stratigraphy and Sedimentology of Quaternary Carbonate Units Around and Within Dean's Blue Hole, Long Island, Bahamas (M.S. Thesis)*. University of Geneva, p. 103.
- Vimpere, L., Del Piero, N., Shawwa, N.A., Beguelin, K., Kindler, P., Castelltort, S., 2021. Upper Pleistocene parabolic ridges (i.e. ‘chevrons’) from The Bahamas: storm-wave sediments or aeolian deposits? A quantitative approach. *Sedimentology* 68, 1255–1288. <https://doi.org/10.1111/sed.12828>.
- Vimpere, L., Kindler, P., Castelltort, S., 2019. Chevrons: origin and relevance for the reconstruction of past wind regimes. *Earth Sci. Rev.* 193, 317–332. <https://doi.org/10.1016/j.earscirev.2019.04.005>.
- Walker, M.J.C., Berkelhammer, M., Björck, S., Cwynar, L.C., Fisher, D.A., Long, A.J., Lowe, J.J., Newnham, R.M., Rasmussen, S.O., Weiss, H., 2012. Formal subdivision of the Holocene Series/Epoch: a discussion paper by a working group of INTIMATE (integration of ice-core, marine and terrestrial records) and the Subcommission on Quaternary Stratigraphy (International Commission on Stratigraphy). *J. Quat. Sci.* 27, 649–659. <https://doi.org/10.1002/jqs.2565>.
- Ward, W.C., Brady, M.J., 1979. Strandline sedimentation of carbonate grainstones, Upper Pleistocene, Yucatan Peninsula, Mexico. *AAPG (Am. Assoc. Pet. Geol.) Bull.* 63, 362–369. <https://doi.org/10.1306/C1EA5616-16C9-11D7-8645000102C1865D>.
- Wessel, B., Huber, M., Wohlfart, C., Marschalk, U., Kosmann, D., Roth, A., 2018. Accuracy assessment of the global TanDEM-X Digital Elevation Model with GPS data. *ISPRS J. Photogrammetry Remote Sens.* 139, 171–182. <https://doi.org/10.1016/j.isprsjprs.2018.02.017>.
- Whitacre, K.E., Kaufman, D.S., Kosnik, M.A., Hearty, P.J., 2017. Converting A/I values (ion exchange) to D/L values (reverse phase) for amino acid geochronology. *Quat. Geochronol.* 37, 1–6. <https://doi.org/10.1016/j.quageo.2016.10.004>.
- Wilson, M.A., Curran, H.A., White, B., 1998. Paleontological evidence of a brief global sea-level event during the last interglacial. *Lethaia* 31, 241–250. <https://doi.org/10.1111/j.1502-3931.1998.tb00513.x>.